On Secure NOMA-CDRT Systems with Physical Layer Network Coding

Hongjiang Lei, Xusheng She, Ki-Hong Park, Imran Shafique Ansari, Zheng Shi, Jing Jiang, and Mohamed-Slim Alouini

arXiv:2205.12591v1 [cs.IT] 25 May 2022

Abstract

This paper proposes a new scheme to enhance the secrecy performance of a NOMA-based coordinated direct relay transmission system (NOMA-CDRT) with an untrusted relay. The physical-layer network coding and the non-orthogonal multiple access scheme are combined to improve the spectrum efficiency. Furthermore, the inter-user interference and friendly jamming signals are utilized to suppress the eavesdropping ability of the untrusted relay without affecting the acceptance quality of legitimate users. Specifically, the far user in the first slot and the near user in the second slot act as jammers to generate jamming signals to ensure secure transmissions of the confidential signals. We investigate the secrecy performance of the proposed scheme in NOMA-CDRT systems and derive the closed-form expression for the ergodic secrecy sum rate. The asymptotic analysis at high signal-to-noise ratio is performed to obtain more insights. Finally, simulation results are presented to demonstrate the effectiveness of the proposed scheme and the correctness of the theoretical analysis.

Index Terms

Coordinated direct relay transmission, non-orthogonal multiple access, physical layer network coding, physical layer security, ergodic secrecy sum rate.

I. Introduction

A. Backgroud and Related Work

During the past decade, several great technologies have been proposed, such as massive multiple-input multiple-output, millimeter-wave, cognitive radio network, and non-orthogonal

Manuscript received.

multiple access (NOMA), etc., to address a large number of connections with diverse requirements in terms of data rates, latency, and spectral efficiency (SE). Compared with conventional orthogonal multiple access, NOMA support multiple users to simultaneously access the same wireless resources. It resolves massive connectivity requirement and conserves spectrum resources in Internet of Things (IoT) network, which utilizes superimposed coding and successive interference cancellation (SIC) to offer a significant improvement in reliable performance [1], [2].

Cooperative NOMA systems have attracted significant attention since they can extend the NOMA users' coverage and enhance the system performance through diversity technology. There are two architectures for cooperative NOMA systems. A dedicated relay is utilized to forward the signal to far users (FUs) due to the deep fading between the base station and the FUs. The other is the near user (NU) acting as a relay to forward the signals to the FUs based on relaying strategies. A downlink NOMA-based coordinated direct and relay transmission (NOMA-CDRT) systems was introduced, wherein parallel communications between multiple links were allowed [3]. Specifically, the NU does not interfere with the relay forwarding signal in the second slot because the signal for the FU in the first time slot has been decoded with SIC technology. Thus, the relay forwards signals to the FU and the base station simultaneously transmits new signals to the NU. Thus, the higher ergodic sum rate and SE were achieved. Liu *et al.* studied the outage performance of a satellite-assisted NOMA-CDRT system and derived the closed-form expression for the exact and asymptotic outage probability (OP) in [4]. The authors in [5] proposed a new signal-space-diversity-based CDRT scheme to improve the achievable ergodic sum rate of the cooperative NOMA system, in which the in-phase or quadrature component of the signals was superimposed and transmitted. The closed-form expressions for the exact and asymptotic OP were derived and compared with non-CDRT scheme. To enhance SE, Nguyen *et al.* proposed an IoT-based CDRT scheme in which the based station transmits the superimposed signals in the first slot in [6]. The IoT controller node works as a relay to decode and forward the superimposed signals to the FU and IoT user in the second slot. The closed-form and approximate expressions for the OP and ergodic sum-rate were derived.

In [7], the CDRT scheme was utilized in the underlay cognitive NOMA system, and closed-form and asymptotic expressions for the OP of the primary and cognitive users were derived. Thai-Hoc *et al.* considered an underlay NOMA-based CDRT system with imperfect SIC, imperfect channel state information (CSI), and co-channel interference in [8]. They proposed multiple

relay selection schemes to improve the system throughput. The closed-form expressions for the exact OP of both primary and cognitive users and the system throughput were derived. Moreover, a deep learning framework was designed to predict the performance of the considered system. To fully utilize the spectrum resources, Zou *et al.* derived the closed-form expression of the ergodic sum-rate for the device-to-device (D2D)-aided NOMA-CDRT systems in which the relay transmits an additional D2D signal to NU while forwarding FU's signals in the second slot in [9]. The authors in [10] proposed a new spectrum-efficient scheme for the NOMA-CDRT system in which the uplink and downlink transmissions were held simultaneously via physical-layer network coding (PNC) scheme. The analytical expressions for the ergodic sum-rate, energy efficiency, and Jain's fairness index of the system were derived. Based on [10], the decoding condition was considered, and an adaptive forward strategy was proposed to implement bidirectional communication in [11]. The closed-form expressions for the OP, outage throughput, and ergodic sum-rate were derived. Moreover, the power allocation coefficient was optimized to maximize the ergodic sum-rate. Yang *et al.* extended NOMA-CDRT with multiple NUs and a best-NU scheduling scheme in which the NU with minimum OP was selected to forward the signals for the FU in [12]. The closed-form expressions for the exact and asymptotic OP were derived.

Compared with the half-duplex (HD) model, the full-duplex (FD) model overcomes the problem of the limited SE of HD, which can not simultaneously transmit and receive on the same resource block, but at the cost of inevitable self-interference [13]. Si *et al.* studied the performance of the NOMA-CDRT system with an FD relay in [14]. Specifically, the signal for the NU was mapped to an M-ary modulated symbol, and the signal for the FU was mapped to a spatial modulation symbol. Then the SE was improved and the energy consumption was reduced by making full use of the antenna resources at the relay. The analytical expressions for the ergodic rate and bit error rate of the proposed scheme were derived. The performance of the NOMA-CDRT system with both FD and HD protocols and multiple FUs was investigated in [15]. Considering residual self-interference, the analytical expressions for the exact OP and the asymptotic ergodic sum-rate were derived. The results showed that the performance with HD outperformed that with FD in the larger-SNR region and self-interference has a more significant impact on the performance of the NU. The power allocation problem of the NOMA-CDRT system was investigated and the optimal closed-form power allocation policies under the HD and FD protocols were derived in [16]. Then, an adaptive relaying scheme was designed to

maximize the minimum user achievable rate.

The parallel transmission between multiple links enhances SE and throughput but makes the secrecy performance analysis more complicated and challenging. Lv *et al.* [17] studied the secrecy performance of a NOMA-CDRT system with an untrusted relay in both uplink and downlink scenarios. Two novel interference-assisted jamming schemes were proposed in which the inter-user interference and the jamming signals were intelligently designed to suppress the reception quality at the relay. The analytical expressions for the lower bound of the exact and asymptotic ergodic secrecy sum-rate (ESSR) were derived. New adaptive jamming schemes were proposed to enhance the secrecy performance of downlink and uplink NOMA-CDRT systems in [18]. The problems of maximizing ESSR through the optimization of the jamming power for both downlink and uplink scenarios were studied. The analytical expressions for the lower bound and asymptotic ESSR were derived. The secrecy performance of a NOMA-CDRT system with multiple NUs was investigated in [19] and the best-user scheduling in which the NU with maximum SNR was selected was proposed to enhance the security. The analytical expressions for the lower bound of the exact and asymptotic ergodic secrecy rate (ESR) were derived.

B. Motivation and Contributions

The PNC scheme improves system throughput while increasing the risk of information eavesdropping. The CDRT scheme improves system throughput with limited SE. However, the research on the security performance of the CDRT systems with the PNC scheme is still in its infancy. This work considers a joint uplink-downlink NOMA-CDRT system with two legitimate users and an untrusted relay, utilizing friendly jammer signals and inter-user interference to provide secure transmission. The main contributions of this paper are summarized as follows.

1) A new scheme, termed as NOMA-CDRT-PNC, is proposed to enhance the secrecy performance of a CDRT with an untrusted relay in which both PNC and NOMA schemes are utilized to improve the spectrum efficiency. The inter-user interference and friendly jamming signals are utilized to suppress the eavesdropping ability of untrusted relay without affecting the SINR of legitimate signals. Specifically, the FU in the first slot and the NU in the second slot work as jammers to transmit jamming signals to ensure secure transmission of the confidential signals.
2) We investigate the secrecy performance of the considered CDRT system and derive the closed-form expression for the lower bound of exact and asymptotic ESSR. Simulation

results are presented to prove the accuracy of the derived analytical expressions.

3) Relative to [10] and [11], in which the PNC scheme with a trusted relay was utilized to enhance SE and outage performance and ergodic sum-rate were investigated, we studied the secrecy performance and the closed-form expression for the lower bound of exact and asymptotic ESSR. Relative to [17] and [18], in which two interference-assisted jamming schemes were proposed for the downlink and uplink CDRT, we proposed a new jamming scheme combined with PNC for the scenarios with downlink and uplink transmissions to improve both secrecy performance and SE simultaneously.

C. Organization

The rest of this paper is organized as follows. Section II describes the system model. In Section III, the analytical expressions for the exact ESSR of NOMA-CDRT-PNC system are derived and analyzed. Asymptotic ESSR of NOMA-CDRT-PNC system is derived to gain more insight in Sections IV. Section V presents the numerical and simulation results to demonstrate the analysis of the security performance of this system and the paper is concluded in Section VI.

II. System Model

Fig. 1 illustrates the system model consisting of a base station denoted by S, a NU denote by U_N, and a FU denote by U_F. There is no direct link between S and U_F due to deep fading and shadowing, then communication link between S and U_F must be deployed via an intermediate relay R, which is trusted at the service level while untrusted at the data level [18], [20]. In other words, R is a potential eavesdropping node to eavesdrop on the confidential information for U_i $(i \in \{N, F\})$. The average channel gains and channel coefficient between source i and destination j are denoted by λ_{ij} and h_{ij} for $i, j \in \{S, U_N, U_F, R\}$ $(i \neq j)$. All the wireless links are assumed to experience quasi-static independent Rayleigh fading and reciprocal. The transmit power at S is denoted as P_S and the transmit power at U_N, U_F, R are denoted as P_U. The data transmission in each fading block has three consecutive and equal phases, as elaborated below.

In the first time slot (t_1), according to downlink NOMA scheme, S broadcasts a superimposed

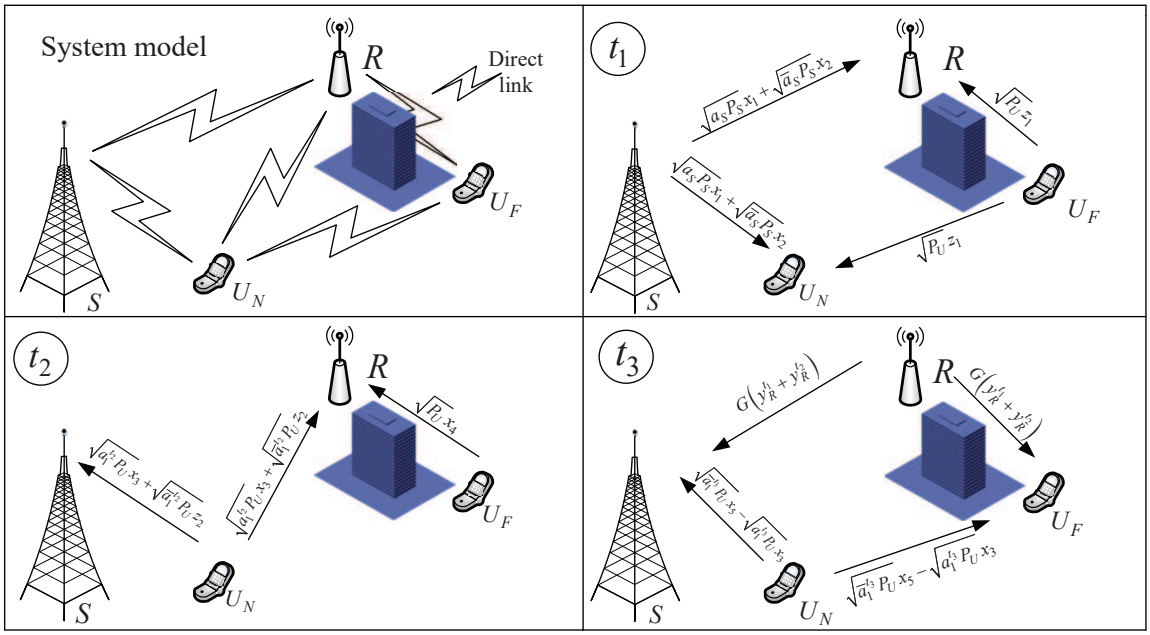


Fig. 1: System model consisting of a base station (S), two users (U_N and U_F), and an untrusted relay (R).

signal of x_1 and x_2 to U_N and U_F. At the same time, U_F sends a jamming signal z_1[1] to effectively disrupt the eavesdropping quality of R. Then the received signals at the destination d is expressed as

$$y_d^{t_1} = h_{Sd}\left(\sqrt{a_S P_S}x_1 + \sqrt{\bar{a}_S P_S}x_2\right) + h_{U_F d}\sqrt{P_U}z_1 + n_d^{t_1}, \tag{1}$$

where $d \in \{U_N, R\}$, a_S denotes the power allocation coefficient for x_1, $\bar{a}_S = 1 - a_S$, and $n_d^{t_1}$ signifies the additive Gaussian white noise (AWGN) in slot t_1. After deleting z_1 and utilizing perfect SIC detection following the decoding order of $x_2 \to x_1$ base on transmit power [3], the SNR of x_1 at U_N is expressed as

$$\gamma^{x_1} = a_S \rho_S |h_{SU_N}|^2, \tag{2}$$

where $\rho_S = \frac{P_S}{\sigma^2}$ and σ^2 signifies the noise power.

[1]In this work, it is assumed that the jamming signals is able to be a Gaussian pseudo-random sequence, or utilizes deterministic waveforms similar to the structure of the desired signal as [20], [21], [22]. Then all the jamming signals are known for the legitimate receivers and the transmitter, which means that the jamming signals do not affect the receiving quality of the legitimate users.

Remark 1. *It must be noted there is a premise for the CDRT system that U_N firstly decode the signal for U_F. which denotes that the power allocation coefficient for x_2 should be greater than 0.5 ($a_S < 0.5$). It is assumed $\lambda_{SR} < \lambda_{SU_N}$ to ensure that U_N firstly decodes U_F signal and then cancel it, which is a premise for the CDRT system.*

It is assumed that R acts as a potential eavesdropper to decode confidential information based on parallel interference cancellation (PIC) technology [18]. The SINRs of x_1 and x_2 at R is obtained as

$$\gamma_R^{x_1} = \frac{a_S \rho_S |h_{SR}|^2}{\bar{a}_S \rho_S |h_{SR}|^2 + \rho_U |h_{U_F R}|^2 + 1}, \tag{3}$$

and

$$\gamma_R^{x_2} = \frac{\bar{a}_S \rho_S |h_{SR}|^2}{a_S \rho_S |h_{SR}|^2 + \rho_U |h_{U_F R}|^2 + 1}, \tag{4}$$

respectively, where $\rho_U = \frac{P_U}{\sigma^2}$.

In the second time slot (t_2), U_N broadcasts a superimposed signal of the desired signal x_3 and a jamming signal z_2 to S and R, U_F synchronously sends its signal x_4 to S. Then the received signals at S and R are expressed as

$$y_S^{t_2} = h_{SU_N} \left(\sqrt{a_1^{t_2} P_U} x_3 + \sqrt{\bar{a}_1^{t_2} P_U} z_2 \right) + n_S^{t_2}, \tag{5}$$

$$y_R^{t_2} = h_{U_N R} \left(\sqrt{a_1^{t_2} P_U} x_3 + \sqrt{\bar{a}_1^{t_2} P_U} z_2 \right) + h_{U_F R} \sqrt{P_U} x_4 + n_R^{t_2}, \tag{6}$$

respectively, where $a_1^{t_2}$ denotes the power allocation for x_3, $\bar{a}_1^{t_2} = 1 - a_1^{t_2}$. After canceling z_2, the SNR of x_3 at S is written as

$$\gamma^{x_3} = a_1^{t_2} \rho_U |h_{SU_N}|^2. \tag{7}$$

With PIC method, the SINRs of x_3 and x_4 at R are expressed as

$$\gamma_R^{x_3} = \frac{\rho_U a_1^{t_2} |h_{U_N R}|^2}{\rho_U \bar{a}_1^{t_2} |h_{U_N R}|^2 + \rho_U |h_{U_F R}|^2 + 1}, \tag{8}$$

and

$$\gamma_R^{x_4} = \frac{\rho_U |h_{U_F R}|^2}{\rho_U |h_{U_N R}|^2 + 1}, \tag{9}$$

respectively.

In the third time slot (t_3), R amplifies the received signals and then broadcasts them with power P_U. Simultaneously, U_N transmits superimposed signals of a new signal x_5 and x_3 to S and R. It should be noted that x_5 can not be wiretapped by R since R is transmitting then

achieve prefect secrecy transmission. Transmitting x_3 aims to linearly eliminate the interference of the forwarded signal from R at U_F. The received signals at S is expressed as

$$\begin{aligned} y_S^{t_3} &= h_{SU_N}\left(\sqrt{\bar{a}_1^{t_3}P_U}x_5 - \sqrt{a_1^{t_3}P_U}x_3\right) + Gh_{SR}\left(y_R^{t_1} + y_R^{t_2}\right) + n_S^{t_3} \\ &= Gh_{SR}h_{SR}\left(\sqrt{a_S P_S}x_1 + \sqrt{\bar{a}_S P_S}x_2\right) + \left(Gh_{SR}h_{U_N R}\sqrt{a_1^{t_2}P_U} - h_{SU_N}\sqrt{a_1^{t_3}P_U}\right)x_3 \\ &+ Gh_{SR}h_{U_F R}\sqrt{P_U}x_4 + h_{SU_N}\sqrt{\bar{a}_1^{t_3}P_U}x_5 + Gh_{SR}h_{U_F R}\sqrt{P_U}z_1 \\ &+ Gh_{SR}h_{U_N R}\sqrt{\bar{a}_1^{t_2}P_U}z_2 + Gh_{SR}n_R^{t_1} + Gh_{SR}n_R^{t_2} + n_S^{t_3} \\ &\overset{(a)}{=} Gh_{SR}h_{U_F R}\sqrt{P_U}x_4 + h_{SU_N}\sqrt{\bar{a}_1^{t_3}P_U}x_5 + n_S, \end{aligned} \tag{10}$$

where $G^2 = \frac{\rho_U}{\rho_S\lambda_{SR}+2\rho_U\lambda_{RU_F}+\rho_U\lambda_{RU_N}+2}$ denotes amplifying coefficient in fixed-gain relay scheme [17], [18], [20], $n_S = Gh_{SR}n_R^{t_1} + Gh_{SR}n_R^{t_2} + n_S^{t_3}$, $a_1^{t_3}$ denotes the power allocation coefficient for x_3, $\bar{a}_1^{t_3} = 1 - a_1^{t_3}$, and step (a) is obtained since x_1, x_2, x_3, z_1, and z_2 are known at S. Then S uses SIC technology following the decoding order of $x_5 \to x_4$ and based on average channel gain of $\lambda_{SR} < \lambda_{SU_N}$ [18], the SINRs of x_5 and x_4 at S are obtained as

$$\gamma^{x_5} = \frac{\bar{a}_1^{t_3}\rho_U|h_{SU_N}|^2}{G^2|h_{SR}|^2\left(\rho_U|h_{U_F R}|^2 + 2\right) + 1}, \tag{11}$$

and

$$\gamma^{x_4} = \frac{G^2\rho_U|h_{SR}|^2|h_{U_F R}|^2}{2G^2|h_{SR}|^2 + 1}, \tag{12}$$

respectively.

Similarly, the received signals at U_F is expressed as

$$\begin{aligned} y_{U_F}^{t_3} &= h_{U_N U_F}\left(\sqrt{\bar{a}_1^{t_3}P_U}x_5 - \sqrt{a_1^{t_3}P_U}x_3\right) + Gh_{RU_F}\left(y_R^{t_1} + y_R^{t_2}\right) + n_{U_F}^{t_3} \\ &\overset{(b)}{=} Gh_{SR}h_{RU_F}\left(\sqrt{a_S P_S}x_1 + \sqrt{\bar{a}_S P_S}x_2\right) + \omega_0 x_3 + h_{U_N U_F}\sqrt{\bar{a}_1^{t_3}P_U}x_5 + n_2, \end{aligned} \tag{13}$$

where $\omega_0 = G\left|h_{RU_F}\right|\left|h_{RU_N}\right|\sqrt{a_1^{t_2}\rho_U} - \left|h_{U_N U_F}\right|\sqrt{a_1^{t_3}\rho_U}$, $n_F = Gh_{RU_F}n_R^{t_1} + Gh_{RU_F}n_R^{t_2} + n_{U_F}^{t_3}$, step (b) is obtained since x_4, z_1, and z_2 are known at U_F. To remove x_3 at U_F, $a_1^{t_3}$ must satisfy $\omega_0 = 0$ Then, we have

$$a_1^{t_3} = \frac{G^2|h_{RU_F}|^2|h_{U_N R}|^2 a_1^{t_2}}{|h_{U_N U_F}|^2}. \tag{14}$$

Taking the expectation operation for $a_1^{t_3}$ [19], we have [2]

$$\begin{aligned}\mathbb{E}\left[a_1^{t_3}\right] &= \frac{G^2 a_1^{t_2}\lambda_{U_N R}\lambda_{RU_F}}{\lambda_{U_N U_F}} \\ &= \frac{\rho_U a_1^{t_2}\lambda_{U_N R}\lambda_{RU_F}}{\lambda_{U_N U_F}\left(\rho_S\lambda_{SR}+2\rho_U\lambda_{RU_F}+\rho_U\lambda_{RU_N}+2\right)} \\ &< \frac{a_1^{t_2}}{\lambda_{U_N U_F}}\frac{\lambda_{U_N R}\lambda_{RU_F}}{\lambda_{RU_F}+\lambda_{RU_N}} \\ &< \frac{\lambda_{U_N R}a_1^{t_2}}{\lambda_{U_N U_F}} \\ &\leq a_1^{t_2} < 1.\end{aligned} \tag{15}$$

It must be noted that $\mathbb{E}\left[a_1^{t_3}\right] < 1$ may not guarantee $a_1^{t_3} < 1$. To meet the causality constraint on power coefficient, we set $a_1^{t_3} = \frac{G^2 a_1^{t_2}\lambda_{U_N R}\lambda_{RU_F}}{\lambda_{U_N U_F}}$. Then U_F uses SIC detection following the decoding order of $x_5 \to x_2$, the SINR of x_2 is obtained as

$$\begin{aligned}\gamma^{x_2} &= \frac{G^2\bar{a}_S\rho_S|h_{SR}|^2|h_{RU_F}|^2}{G^2|h_{RU_F}|^2\left(a_S\rho_S|h_{SR}|^2+2\right)+\omega_0^2+1} \\ &\approx \frac{G^2\bar{a}_S\rho_S|h_{SR}|^2|h_{RU_F}|^2}{G^2|h_{RU_F}|^2\left(a_S\rho_S|h_{SR}|^2+2\right)+1}.\end{aligned} \tag{16}$$

The instantaneous secrecy rate of x_j is expressed as [23]

$$C_s^{x_j} = \left[\ln\left(1+\gamma^{x_j}\right) - \ln\left(1+\gamma_R^{x_j}\right)\right]^+, \tag{17}$$

where $j = 1, \cdots, 5$ and $[x]^+ = \max\{x, 0\}$.

III. Ergodic Secrecy Sum Rate Analysis

In this section, we analyze the ESSR of the proposed NOMA-CDRT-PNC scheme, which is expressed as

$$\begin{aligned}\bar{C}_{\text{ESSR}} &= \sum_{j=1}^{5}\bar{C}_{\text{ESR}}^{x_j} \\ &= \frac{1}{3}\sum_{j=1}^{4}\mathbb{E}\left[C^{x_j} - C_R^{x_j}\right]^+ + \frac{1}{3}\mathbb{E}\left[C^{x_5}\right],\end{aligned} \tag{18}$$

[2]In this work, it is assumed $\lambda_{U_N R} \leq \lambda_{U_N U_F}$ to ensure $\mathbb{E}\left[a_1^{t_3}\right] < 1$.

where $\bar{C}_{\mathrm{ESR}}^{x_j}$ denotes the ergodic secrecy rate of x_j, $C^{x_j}=\ln\left(1+\gamma^{x_j}\right)$, $C_R^{x_j}=\ln\left(1+\gamma_R^{x_j}\right)$, $\mathbb{E}\left[\cdot\right]$ denotes expectation operator. By utilizing Jensen's inequality, the lower bound of the ESSR is expressed as

$$\begin{aligned}\bar{C}_{\mathrm{ESSR}}^{\mathrm{L}}&=\sum_{j=1}^{5}\bar{C}_{\mathrm{ESR}}^{x_j,\mathrm{L}}\\&=\frac{1}{3}\sum_{i=1}^{4}\left[\bar{C}^{x_j}-\bar{C}_R^{x_j}\right]^{+}+\frac{1}{3}\bar{C}^{x_5},\end{aligned}\tag{19}$$

where $\bar{C}^{x_j}=\mathbb{E}\left[C^{x_j}\right]$, $\bar{C}_R^{x_j}=\mathbb{E}\left[C_R^{x_j}\right]$, and the superscript 'L' denotes lower bound. Based on the probability theory, ergodic capacity is expressed as

$$\begin{aligned}\bar{C}&=\mathbb{E}\left[\ln\left(1+\gamma\right)\right]\\&=\int_0^{\infty}\ln\left(1+x\right)f_{\gamma}\left(x\right)dx\\&=\int_0^{\infty}\frac{1-F_{\gamma}\left(x\right)}{1+x}dx,\end{aligned}\tag{20}$$

where $f_{\gamma}\left(x\right)$ and $F_{\gamma}\left(x\right)$ are probability density function (PDF) and cumulative distribution function (CDF) of γ, respectively.

The analytical expressions for ergodic rate of all the signals in Section II are derived as follows.

Substituting (2) into (20) and utilizing [24, (4.337.2)], $\bar{C}^{x_1}$ is obtained as

$$\begin{aligned}\bar{C}^{x_1}&=\mathbb{E}\left[\ln\left(1+a_S\rho_S|h_{SU_N}|^2\right)\right]\\&=\frac{1}{\lambda_{SU_N}}\int_0^{\infty}\ln\left(1+a_S\rho_S x\right)e^{-\frac{x}{\lambda_{SU_N}}}dx\\&=\phi_1\left(a_S\rho_S\lambda_{SU_N}\right),\end{aligned}\tag{21}$$

where $\phi_1\left(x\right)=-\exp\left(\frac{1}{x}\right)\mathrm{Ei}\left(-\frac{1}{x}\right)$ and $\mathrm{Ei}\left(x\right)=-\int_{-x}^{\infty}t^{-1}\exp\left(-t\right)dt$ is exponential integral function, defined by [24, (8.211.1)].

Based on (3), we obtain the CDF of $\gamma_R^{x_1}$ as

$$\begin{aligned} F_{\gamma_R^{x_1}}(x) &= \Pr\left\{\frac{a_S\rho_S|h_{SR}|^2}{\bar{a}_S\rho_S|h_{SR}|^2+\rho_U|h_{U_FR}|^2+1}<x\right\} \\ &= \begin{cases} \Pr\left\{|h_{SR}|^2<\frac{\rho_U x|h_{U_FR}|^2+x}{(a_S-\bar{a}_S x)\rho_S}\right\}, & x<\frac{a_S}{\bar{a}_S}, \\ 1, & x>\frac{a_S}{\bar{a}_S}, \end{cases} \\ &= \begin{cases} \int_0^\infty F_{|h_{SR}|^2}\left(\frac{\rho_U xy+x}{(a_S-\bar{a}_S x)\rho_S}\right) f_{|h_{RU_F}|^2}(y)\,dy, & x<\frac{a_S}{\bar{a}_S}, \\ 1, & x>\frac{a_S}{\bar{a}_S}, \end{cases} \\ &= \begin{cases} 1-\frac{a_S-\bar{a}_S x}{(\omega_1-\bar{a}_S)x+a_S}e^{-\frac{x}{\rho_S\lambda_{SR}(a_S-\bar{a}_S x)}}, & x<\frac{a_S}{\bar{a}_S}, \\ 1, & x>\frac{a_S}{\bar{a}_S}, \end{cases} \end{aligned} \tag{22}$$

where $\omega_1=\frac{\rho_U\lambda_{RU_F}}{\rho_S\lambda_{SR}}$. Substituting (22) into (20) and utilizing [24, (3.352.4)], $\bar{C}_R^{x_1}$ is derived as

$$\begin{aligned} \bar{C}_R^{x_1} &= \int_0^\infty \frac{1}{x+1}\left(1-F_{\gamma_R^{x_1}}(x)\right)dx \\ &= \frac{\phi_2(\rho_S\lambda_{SR},\bar{a}_S\rho_S\lambda_{SR})}{1-\omega_1}-\frac{\omega_1 a_S\phi_2(\omega_1\rho_S\lambda_{SR},\bar{a}_S\rho_S\lambda_{SR})}{(1-\omega_1)(\omega_1-\bar{a}_S)}, \end{aligned} \tag{23}$$

where $\phi_2(a,b)=\phi_1(a)-\phi_1(b)$. Substituting (21) and (23) into (19), the closed-form expression for lower bound of $\bar{C}_{\mathrm{ESR}}^{x_1}$ is obtained.

Remark 2. *Based on (2) and (3), one can find that both γ^{x_1} and $\gamma_R^{x_1}$ increase as increasing of a_S. However, increasing of γ^{x_1} is faster than the increasing of $\gamma_R^{x_1}$ because $\gamma_R^{x_1}<\frac{a_S\rho_S|h_{SR}|^2}{\rho_U|h_{U_FR}|^2+1}$ and $\gamma^{x_1}=a_S\rho_S|h_{SU_N}|^2$ is proportional to a_S. Thus, The ESR of x_1 increases as increasing a_S.*

The CDF of x_2 is obtained as

$$\begin{aligned} F_{\gamma^{x_2}}(x) &= \Pr\left\{\frac{G^2\bar{a}_S\rho_S|h_{RU_F}|^2|h_{SR}|^2}{G^2|h_{RU_F}|^2\left(a_S\rho_S|h_{SR}|^2+2\right)+1}<x\right\} \\ &= \begin{cases} \Pr\left\{|h_{SR}|^2<\frac{\left(2G^2|h_{RU_F}|^2+1\right)x}{(\bar{a}_S-a_S x)G^2\rho_S|h_{RU_F}|^2}\right\}, & x<\frac{\bar{a}_S}{a_S}, \\ 1, & x>\frac{\bar{a}_S}{a_S}, \end{cases} \\ &= \begin{cases} \int_0^\infty F_{|h_{SR}|^2}\left(\frac{2xy+x/G^2}{\rho_S(\bar{a}_S-a_S x)y}\right) f_{|h_{RU_F}|^2}(y)\,dy, & x<\frac{\bar{a}_S}{a_S}, \\ 1, & x>\frac{\bar{a}_S}{a_S}, \end{cases} \\ &= \begin{cases} 1-\phi_3\left(\frac{x}{\beta_S(\bar{a}_S-a_S x)}\right)e^{-\frac{2x}{\rho_S\lambda_{SR}(\bar{a}_S-a_S x)}}, & x<\frac{\bar{a}_S}{a_S}, \\ 1, & x>\frac{\bar{a}_S}{a_S}, \end{cases} \end{aligned} \tag{24}$$

where $\beta_S = \frac{G^2\rho_S\lambda_{SR}\lambda_{RU_F}}{4}$, $\phi_3(x) = \sqrt{x}K_1(\sqrt{x})$, and $K_v(\cdot)$ is the v-order modified Bessel function of the second kind, defined in [24, (8.432.1)]. Substituting (24) into (20) and utilizing [24, (3.324.1)], we obtain

$$\begin{aligned}\bar{C}^{x_2} &= \int_0^\infty \frac{\beta_S}{\beta_S x+1} e^{-\frac{G^2\lambda_{RU_F}x}{2}} \sqrt{x}K_1\left(\sqrt{x}\right) dx \\ &\quad - \int_0^\infty \frac{a_S\beta_S}{a_S\beta_S x+1} e^{-\frac{G^2\lambda_{RU_F}x}{2}} \sqrt{x}K_1\left(\sqrt{x}\right) dx \\ &= \beta_S\phi_4\left(\beta_S, \frac{G^2\lambda_{RU_F}}{2}\right) - a_S\beta_S\phi_4\left(a_S\beta_S, \frac{G^2\lambda_{RU_F}}{2}\right),\end{aligned} \tag{25}$$

where $\phi_4(a,b) = \int_0^\infty \frac{1}{ax+1} e^{-bx}\sqrt{x}K_1(\sqrt{x})\,dt$. Utilizing [24, (9.34.3)], (10) and (11) of [31], and [26, (1.2)], $\phi_4(a,b)$ is denoted as

$$\begin{aligned}\phi_4(a,b) &= \int_0^\infty \frac{1}{ax+1} e^{-bx}\sqrt{x}K_1\left(\sqrt{x}\right) dt \\ &= \int_0^\infty G_{1,1}^{1,1}\left[ax\left|{}^{0}_{0}\right.\right] G_{0,1}^{1,0}\left[bx\left|{}^{-}_{0}\right.\right] G_{0,2}^{2,0}\left[\frac{x}{4}\left|{}^{-}_{1,0}\right.\right] dx \\ &= \frac{1}{b} H_{0,0:0,0:0,0}^{0,1:1,1:0,2}\left[\begin{matrix}1 \\ -\end{matrix}\middle|\begin{matrix}0 \\ 0\end{matrix}\middle|\begin{matrix}- \\ 1,0\end{matrix}\middle|\frac{a}{b}, \frac{1}{4b}\right],\end{aligned} \tag{26}$$

where $G_{c,d}^{a,b}[\cdot]$ is the Meijer's G-function defined by [24, (9.301)] and $H_{c,d:p,r:a,\beta}^{0,b:m,n:\gamma,\varepsilon}[\cdot]$ is the Extended Generalized Bivariate Fox's H-function (EGBFHF) defined by [26, (2.57)].

With the same method as (23), $\bar{C}_R^{x_2}$ is obtained as

$$\bar{C}_R^{x_2} = \frac{\phi_2(\rho_S\lambda_{SR}, a_S\rho_S\lambda_{SR})}{1-\omega_1} - \frac{\omega_1\bar{a}_S\phi_2(\omega_1\rho_S\lambda_{SR}, a_S\rho_S\lambda_{SR})}{(1-\omega_1)(\omega_1-a_S)}. \tag{27}$$

Substituting (25) and (27) into (20), the closed-form for lower bound of $\bar{C}_{\mathrm{ESR}}^{x_2}$ is obtained.

Remark 3. *Based on (4) and (16), one can find that both γ^{x_2} and $\gamma_R^{x_2}$ tend to a constant independent to ρ at the high-SNR region. Moreover, one can find that the effect of a_S on the ESR of x_2 is the opposite of the effect of a_S on the ESR of x_1 because increasing a_S signifies decreasing of the transmit power for x_2, which lead to the deterioration of the ESR of x_2, testified in [27].*

With the same method as (21) and (23), we obtain $\bar{C}^{x_3}$ and $\bar{C}_R^{x_3}$ as

$$\bar{C}^{x_3} = \phi_1\left(a_1^{t_2}\rho_U\lambda_{SU_N}\right), \tag{28}$$

and

$$\bar{C}_R^{x_3} = \frac{\bar{a}_1^{t_2}\phi_2\left(\bar{a}_1^{t_2}\rho_U\lambda_{RU_N}, \rho_U\lambda_{RU_F}\right)}{\omega_2 - \bar{a}_1^{t_2}} - \frac{\phi_2(\rho_U\lambda_{RU_N}, \rho_U\lambda_{RU_F})}{\omega_2 - 1}, \tag{29}$$

respectively, where $\omega_2 = \frac{\lambda_{RU_F}}{\lambda_{RU_N}}$. Substituting (28) and (29) into (20), the closed-form for lower bound of $\bar{C}_{\mathrm{ESR}}^{x_3}$ is obtained.

Remark 4. *Although the equation of the ESR of x_3 is similar to that of the ESR of x_1, it must be noted that the effect of $a_1^{t_2}$ on the ESR of x_3 is different from the effect of a_S on the ESR of x_1 since there is $0 \leq a_1^{t_2} \leq 1$ while $a_S < 0.5$. Based on (8), one can find that increasing means that $a_1^{t_2}$ denotes more power is allocated to x_3 and less power is allocated to z_2, which leads to increasing both $\gamma_R^{x_3}$ and γ^{x_3}. However, $\gamma_R^{x_3}$ at $0.5 < a_1^{t_2} < 1$ region increases faster than that at $0 < a_1^{t_2} < 0.5$ because the power allocated to z_2 tends to zero. Thus the ESR of x_3 increases first and then decreases as $a_1^{t_2}$ increases. Thus, there exists an optimal $a_1^{t_2}$ to maximize the ESR of x_3.*

With the same method as (24), we obtain

$$F_{\gamma^{x_4}}(x) = 1 - e^{-\frac{2x}{\rho_U \lambda_{RU_F}}} \phi_3\left(\frac{x}{\beta_U}\right), \tag{30}$$

where $\beta_U = \frac{G^2 \rho_U \lambda_{SR} \lambda_{RU_F}}{4}$. Similar as (25), we obtain

$$\bar{C}^{x_4} = \beta_U \phi_4\left(\beta_U, \frac{G^2 \lambda_{SR}}{2}\right). \tag{31}$$

The CDF of $\gamma_R^{x_4}$ is expressed as

$$\begin{aligned} F_{\gamma_R^{x_4}}(x) &= \Pr\left\{|h_{U_F R}|^2 < \frac{\rho_U x |h_{U_N R}|^2 + x}{\rho_U}\right\} \\ &= \int_0^\infty F_{|h_{RU_F}|^2}\left(\frac{\rho_U x y + x}{\rho_U}\right) f_{|h_{RU_N}|^2}(y)\, dy \\ &= 1 - \frac{\lambda_{RU_F}}{\lambda_{RU_N} x + \lambda_{RU_F}} e^{-\frac{x}{\rho_U \lambda_{RU_F}}}. \end{aligned} \tag{32}$$

Substituting (32) into (20), utilizing [24, (3.352.4)], we obtain

$$\begin{aligned} \bar{C}_R^{x_4} &= \int_0^\infty \frac{1}{x+1}\left(1 - F_{\gamma_R^{x_4}}(x)\right) dx \\ &= \int_0^\infty \frac{1}{x+1} \frac{\lambda_{RU_F}}{\lambda_{RU_N} x + \lambda_{RU_F}} e^{-\frac{x}{\rho_U \lambda_{RU_F}}} dx \\ &= \frac{\omega_2 \phi_2\left(\rho_U \lambda_{RU_F}, \rho_U \lambda_{RU_N}\right)}{\omega_2 - 1}. \end{aligned} \tag{33}$$

Substituting (31) and (33) into (20), the closed-form for lower bound of $\bar{C}_{\mathrm{ESR}}^{x_4}$ is obtained.

Based on (11), the CDF of x_5 is obtained as

$$\begin{aligned} F_{\gamma^{x_5}}(x) &= \Pr\left\{|h_{SU_N}|^2 < \frac{G^2|h_{SR}|^2 x\left(\rho_U|h_{RU_F}|^2+2\right)+x}{\bar{a}_1^{t_3}\rho_U}\right\} \\ &= \int_0^\infty \int_0^\infty F_{|h_{SU_N}|^2}\left(\frac{G^2xy\left(\rho_U z+2\right)+x}{\bar{a}_1^{t_3}\rho_U}\right) f_{|h_{SR}|^2}(y)\, f_{|h_{RU_F}|^2}(z)\, dydz \\ &= 1-\frac{\bar{a}_1^{t_3}\lambda_{SU_N}}{G^2\lambda_{SR}\lambda_{RU_F}x} e^{-\frac{x}{\bar{a}_1^{t_3}\rho_U\lambda_{SU_N}}}\phi_1\left(\frac{2}{\rho_U\lambda_{RU_F}}+\frac{\bar{a}_1^{t_3}\lambda_{SU_N}}{G^2\lambda_{SR}\lambda_{RU_F}x}\right). \end{aligned} \tag{34}$$

Then the ergodic rate of x_5 is expressed as

$$\bar{C}^{x_5} = \frac{\bar{a}_1^{t_3}\lambda_{SU_N}}{G^2\lambda_{SR}\lambda_{RU_F}}\int_0^\infty \frac{1}{x\left(x+1\right)} e^{-\frac{x}{\bar{a}_1^{t_3}\rho_U\lambda_{SU_N}}}\phi_1\left(\frac{2}{\rho_U\lambda_{RU_F}}+\frac{\bar{a}_1^{t_3}\lambda_{SU_N}}{G^2\lambda_{SR}\lambda_{RU_F}x}\right)dx. \tag{35}$$

The closed-form expression for (35) is difficult to obtain since there is a complicated integral of exponential integral function, then its lower bound is derived based on the method proposed in [19]. We define $X=\bar{a}_1^{t_3}\rho_U|h_{SU_N}|^2$ and $Y=G^2|h_{SR}|^2\left(\rho_U|h_{RU_F}|^2+2\right)$, and using Jensen's inequality, we obtain

$$\begin{aligned} C^{x_5} &= \mathbb{E}\left[\ln\left(1+\gamma^{x_5}\right)\right] \\ &= \mathbb{E}\left[\ln\left(1+\frac{X}{1+Y}\right)\right] \\ &= \mathbb{E}\left[\ln\left(1+e^{\ln\left(\frac{X}{1+Y}\right)}\right)\right] \\ &\geq C^{x_5,\mathrm{L}} = \ln\left(1+e^{\mathbb{E}\left[\ln\left(\frac{X}{1+Y}\right)\right]}\right) \\ &= \ln\left(1+\mathrm{e}^{\Phi}\right), \end{aligned} \tag{36}$$

where $\Phi=\mathbb{E}\left[\ln\left(X\right)\right]-\mathbb{E}\left[\ln\left(1+Y\right)\right]$. Utilizing [24, (4.311.1)], we have

$$\begin{aligned} \mathbb{E}\left[\ln\left(X\right)\right] &= \int_0^\infty \ln\left(\bar{a}_1^{t_3}\rho_U x\right) f_{|h_{SU_N}|^2}(x)\, dx \\ &= \ln\left(\bar{a}_1^{t_3}\rho_U\lambda_{SU_N}\right)-\mathrm{C}, \end{aligned} \tag{37}$$

where $\mathrm{C}=0.577215$ denotes Euler's constant [24, (8.367.1)]. By utilizing

$$\int_{x_0}^{x_1} e^{-ax-\frac{b}{x}}dx \approx \left(e^{-ax_0}-e^{-ax_1}\right)\sqrt{\frac{4b}{a}}K_1\left(\sqrt{4ab}\right), \tag{38}$$

which is verified in [28], the CDF of Y is obtained as

$$\begin{aligned} F_Y(y) &= \Pr\left\{|h_{SR}|^2 < \frac{y}{G^2\left(\rho_U|h_{RU_F}|^2+2\right)}\right\} \\ &= \int_0^\infty F_{|h_{SR}|^2}\left(\frac{y}{G^2(\rho_U x+2)}\right) f_{|h_{RU_F}|^2}(x)\,dx \\ &= 1-\frac{1}{\lambda_{RU_F}}\int_0^\infty e^{-\frac{y}{G^2\lambda_{SR}(\rho_U x+2)}} e^{-\frac{x}{\lambda_{RU_F}}}\,dx \\ &= 1-\frac{1}{\rho_U\lambda_{RU_F}} e^{\frac{2}{\rho_U\lambda_{RU_F}}}\int_2^\infty e^{-\frac{y}{G^2\lambda_{SR}t}} e^{-\frac{t}{\rho_U\lambda_{RU_F}}}\,dt \\ &\approx 1-\phi_3\left(\frac{y}{\beta_U}\right). \end{aligned} \tag{39}$$

Substituting (39) into (20), utilizing [24, (9.31.2)] and [31, (21)], we obtain

$$\begin{aligned} &\mathbb{E}\left[\ln(1+Y)\right] \\ &= \int_0^\infty \frac{1-F_Y(x)}{1+x}dx \\ &= \beta_U\int_0^\infty G_{1,1}^{1,1}\left[\beta_U t\,\middle|_0^0\right] G_{0,2}^{2,0}\left[\frac{t}{4}\,\middle|_{1,0}^{-}\right] dt \\ &= G_{1,3}^{3,1}\left[\frac{1}{4\beta_U}\,\middle|_{1,0,0}^{0}\right]. \end{aligned} \tag{40}$$

Then, we have

$$\Phi = \ln\left(\bar{a}_1^{t_3}\rho_U\lambda_{SU_N}\right) - G_{1,3}^{3,1}\left[\frac{1}{4\beta_U}\,\middle|_{1,0,0}^{0}\right] - \mathrm{C}. \tag{41}$$

Substituting (41) into $C^{x_5,\mathrm{L}}$, the closed-form for lower bound of $\bar{C}_{\mathrm{ESR}}^{x_5}$ is obtained.

Remark 5. *Based on $a_1^{t_3} = \frac{G^2 a_1^{t_2}\lambda_{U_N R}\lambda_{RU_F}}{\lambda_{U_N U_F}}$, one can find that increasing $a_1^{t_2}$ signifies decreasing of $\bar{a}_1^{t_3}$ and $\bar{C}_{\mathrm{ESR}}^{x_5}$ since the transmit power for x_5, which lead to the deterioration of the ESR of x_5.*

Substituting (21), (23), (25), (27), (28), (29), (31), (33), and (36) into (19), the analytical

expressions for the lower bound of the ESSR is obtained as

$$\begin{aligned}\bar{C}_{\mathrm{ESSR}}^{\mathrm{L}} = & \frac{1}{3}\left[\phi_1\left(a_S\rho_S\lambda_{SU_N}\right) - \frac{\phi_2\left(\rho_S\lambda_{SR}, \bar{a}_S\rho_S\lambda_{SR}\right)}{1-\omega_1} + \frac{\omega_1 a_S \phi_2\left(\omega_1\rho_S\lambda_{SR}, \bar{a}_S\rho_S\lambda_{SR}\right)}{\left(1-\omega_1\right)\left(\omega_1-\bar{a}_S\right)}\right]^+ \\ & + \frac{1}{3}\left[\beta_S\phi_4\left(\beta_S, \frac{G^2\lambda_{RU_F}}{2}\right) - a_S\beta_S\phi_4\left(a_S\beta_S, \frac{G^2\lambda_{RU_F}}{2}\right) - \frac{\phi_2\left(\rho_S\lambda_{SR}, a_S\rho_S\lambda_{SR}\right)}{1-\omega_1}\right. \\ & \left. + \frac{\omega_1\bar{a}_S\phi_2\left(\omega_1\rho_S\lambda_{SR}, a_S\rho_S\lambda_{SR}\right)}{\left(1-\omega_1\right)\left(\omega_1-a_S\right)}\right]^+ \\ & + \frac{1}{3}\left[\phi_1\left(a_1^{t_2}\rho_U\lambda_{SU_N}\right) + \frac{\phi_2\left(\rho_U\lambda_{RU_N}, \rho_U\lambda_{RU_F}\right)}{\omega_2-1} - \frac{\bar{a}_1^{t_2}\phi_2\left(\bar{a}_1^{t_2}\rho_U\lambda_{RU_N}, \rho_U\lambda_{RU_F}\right)}{\omega_2-\bar{a}_1^{t_2}}\right]^+ \\ & + \frac{1}{3}\left[\beta_U\phi_4\left(\beta_U, \frac{G^2\lambda_{SR}}{2}\right) - \frac{\omega_2\phi_2\left(\rho_U\lambda_{RU_F}, \rho_U\lambda_{RU_N}\right)}{\omega_2-1}\right]^+ + \frac{1}{3}\ln\left(1+e^{\Phi}\right).\end{aligned} \tag{42}$$

The analytical expressions is complicated because many factors affect the ESSR of the considered system, specifically, the power coefficients $\left(a_S, a_1^{t_2}\right)$, the transmit powers (P_S, P_U), and the average channel gains $(\lambda_{SU_N}, \lambda_{SR}, \lambda_{U_NR}, \lambda_{RU_F}, \lambda_{U_NU_F})$. To obtain more insights, we derive asymptotic expressions of the ESSR in the high transmit power regime in the next section.

IV. Asymptotic Analysis for Ergodic Secrecy Sum Rate

To gain more insights about the proposed scheme, we analyze asymptotic ESSR expression in high-SNR region in this section. It assumed $\rho_S = \nu\rho_U$ and $\rho_U = \rho \to \infty$.

Based on (21), utilizing $\mathrm{Ei}\left(x\right) \overset{x\to 0^-}{\sim} \mathrm{C} + \ln\left(-x\right)$ and $e^x \overset{x\to 0}{\sim} 1+x$[29], we have $\phi_1\left(x\right) \overset{x\to 0}{\approx} \ln\left(x\right) - \mathrm{C}$. Then the asymptotic ESR of x_1 is obtained as

$$\begin{aligned}\bar{C}_{\mathrm{ESR}}^{x_1,\rho\to\infty} &= \bar{C}^{x_1,\rho\to\infty} - \bar{C}_R^{x_1,\rho\to\infty} \\ &= \ln\left(a_S\nu\rho\lambda_{SU_N}\right) + \frac{\omega_1 a_S\ln\left(\omega_1\right)}{\left(1-\omega_1\right)\left(\omega_1-\bar{a}_S\right)} - \frac{\bar{a}_S\ln\left(\bar{a}_S\right)}{\omega_1-\bar{a}_S} - \mathrm{C} \\ &\approx \ln\left(a_S\nu\rho\lambda_{SU_N}\right).\end{aligned} \tag{43}$$

Similarly, the asymptotic ESR of x_3 is obtained as

$$\begin{aligned}\bar{C}_{\mathrm{ESR}}^{x_3,\rho\to\infty} &= \bar{C}^{x_3,\rho\to\infty} - \bar{C}_R^{x_3,\rho\to\infty} \\ &= \ln\left(a_1^{t_2}\rho\lambda_{SU_N}\right) + \frac{\omega_2 a_1^{t_2}\ln\left(\omega_2\right)}{\left(1-\omega_2\right)\left(\omega_2-\bar{a}_1^{t_2}\right)} - \frac{\bar{a}_1^{t_2}\ln\left(\bar{a}_1^{t_2}\right)}{\omega_2-\bar{a}_1^{t_2}} - \mathrm{C} \\ &\approx \ln\left(a_1^{t_2}\rho\lambda_{SU_N}\right).\end{aligned} \tag{44}$$

Remark 6. *Based on (43) and (44), one can observer that the lower bounds of ESR of x_1 and x_3 scale as $\ln\left(\rho\right)$ at high-SNR region. This is because SIC deletes the inter-user interference*

on U_N and the jamming signal does not affect γ^{x_1} and γ^{x_3}, which tends to infinity as $\rho \to \infty$. However, the inter-user interference and the jamming signal on R can not be deleted by PIC, then $\gamma_R^{x_1}$ and $\gamma_R^{x_3}$ tend to be a constant, which is independent of ρ. Moreover, the asymptotic ESR of x_1 is proportional to a_S, which is same as statement in Remark 2.

Utilizing $K_1(x) \overset{x\to 0}{\approx} \frac{1}{x} + \frac{x}{2}\ln\left(\frac{x}{2}\right)$ [30, (17)], we have $xK_1(x) \overset{x\to 0}{\approx} 1 + \frac{x^2}{2}\ln\left(\frac{x}{2}\right) \approx 1$, then $\bar{C}_R^{x_4}$ is approximated as

$$\bar{C}^{x_4,\rho\to\infty} = e^{\frac{2}{\rho\lambda_{RU_F}}}\left(\ln\left(\frac{\rho\lambda_{RU_F}}{2}\right) - \mathrm{C}\right). \tag{45}$$

With the same method as (43), we have

$$\bar{C}_R^{x_4,\rho\to\infty} = \frac{\omega_2}{\omega_2 - 1}\ln(\omega_2), \tag{46}$$

Then the asymptotic ESR of x_4 is obtained as

$$\begin{aligned}\bar{C}_{\mathrm{ESR}}^{x_4,\rho\to\infty} &= e^{\frac{2}{\rho\lambda_{RU_F}}}\left(\ln\left(\frac{\rho\lambda_{RU_F}}{2}\right) - \mathrm{C}\right) - \frac{\omega_2}{\omega_2 - 1}\ln(\omega_2) \\ &\approx \ln\left(\frac{\rho\lambda_{RU_F}}{2}\right).\end{aligned} \tag{47}$$

Remark 7. *Based on (47), one can observe that the lower bound of ESR of x_4 scales as $\ln(\rho)$ at the high-SNR region.*

Based on (25), utilizing $K_1(x) \overset{x\to 0}{\approx} \frac{1}{x} + \frac{x}{2}\ln\left(\frac{x}{2}\right)$ [30, (17)], $\bar{C}^{x_2}$ is approximated as

$$\begin{aligned}\bar{C}^{x_2,\rho\to\infty} = &\underbrace{\int_0^\infty \frac{1}{x + \frac{1}{\beta_S}} e^{-\frac{G^2\lambda_{RU_F}x}{2}}\left(1 + \frac{x}{4}\ln\left(\frac{x}{4}\right)\right)dx}_{\triangleq I_1} \\ &- \underbrace{\int_0^\infty \frac{1}{x + \frac{1}{a_S\beta_S}} e^{-\frac{G^2\lambda_{RU_F}x}{2}}\left(1 + \frac{x}{4}\ln\left(\frac{x}{4}\right)\right)dx}_{\triangleq I_2}.\end{aligned} \tag{48}$$

Utilizing [24, (3.352.4), (4.331.1)], we obtain I_1 as

$$\begin{aligned}I_1 &= \int_0^\infty \frac{1}{x + \frac{1}{\beta_S}} e^{-\frac{G^2\lambda_{RU_F}x}{2}}dx + \frac{1}{4}\int_0^\infty \left(1 - \frac{\frac{1}{\beta_S}}{x + \frac{1}{\beta_S}}\right) e^{-\frac{G^2\lambda_{RU_F}x}{2}}\ln\left(\frac{x}{4}\right)dx \\ &= \phi_1\left(\frac{2\beta_S}{G^2\lambda_{RU_F}}\right) + \int_0^\infty e^{-2G^2\lambda_{RU_F}y}\ln(y)\,dy - \int_0^\infty \frac{1}{4\beta_S y + 1} e^{-2G^2\lambda_{RU_F}y}\ln(y)\,dy \\ &= \phi_1\left(\frac{\nu\rho\lambda_{SR}}{2}\right) - \frac{\mathrm{C} + \ln\left(2G^2\lambda_{RU_F}\right)}{2G^2\lambda_{RU_F}} - \phi_5\left(4\beta_S, 2G^2\lambda_{RU_F}\right),\end{aligned} \tag{49}$$

where $\phi_5(a,b)$ is denoted as

$$\begin{aligned}\phi_5(a,b) &= \int_0^\infty \frac{1}{ay+1}\exp(-by)\ln(y)\,dy \\ &= \frac{1}{2a}\ln\left(\frac{b}{a}\right)\ln(ab) - \frac{\psi^{(1)}(1)}{2a} + \frac{\mathrm{C}\ln(b)}{a} + \frac{\mathrm{C}^2}{2a},\end{aligned} \tag{50}$$

where $\psi^{(k)}(x)$ is the polygamma function, defined by [24, (8.363.8)]. The detailed derivation of $\phi_5(a,b)$ is given in Appendix A. Similarly, we obtain

$$I_2 = \phi_1\left(\frac{a_S\nu\rho\lambda_{SR}}{2}\right) - \frac{\mathrm{C}+\ln(2G^2\lambda_{RU_F})}{2G^2\lambda_{RU_F}} - \phi_5\left(4a_S\beta_S, 2G^2\lambda_{RU_F}\right). \tag{51}$$

Due to $\beta_S = \frac{G^2\rho_S\lambda_{SR}\lambda_{RU_F}}{4} \to \infty$, $\phi_5(a,b) \overset{a\to\infty}{\approx} 0$, $\phi_1(x) \overset{x\to 0}{\approx} \ln(x) - \mathrm{C}$, and $\phi_2(a,b) \overset{a,b\to 0}{\approx} \ln\left(\frac{a}{b}\right)$. Substituting (49) and (51) into (48), we obtain $\bar{C}^{x_2,\rho\to\infty}$ as

$$\begin{aligned}\bar{C}^{x_2,\rho\to\infty} &= \phi_2\left(\frac{\nu\rho\lambda_{SR}}{2}, \frac{a_S\nu\rho\lambda_{SR}}{2}\right) + \phi_5\left(4a_S\beta_S, 2G^2\lambda_{RU_F}\right) - \phi_5\left(4\beta_S, 2G^2\lambda_{RU_F}\right) \\ &\approx \ln\left(\frac{1}{a_S}\right).\end{aligned} \tag{52}$$

Based on (27), utilizing $\phi_1(x) \overset{x\to 0}{\approx} \ln(x) - \mathrm{C}$, $\bar{C}_R^{x_2}$ is approximated as

$$\bar{C}_R^{x_2,\rho\to\infty} = \frac{a_S\ln(a_S)}{\omega_1 - a_S} - \frac{\omega_1\bar{a}_S\ln(\omega_1)}{(1-\omega_1)(\omega_1 - a_S)}. \tag{53}$$

Then the asymptotic ESR of x_2 is obtained as

$$\bar{C}_{\mathrm{ESR}}^{x_2,\rho\to\infty} \approx \frac{\omega_1}{\omega_1 - a_S}\left(\ln\left(\frac{1}{a_S}\right) + \frac{\bar{a}_S\ln(\omega_1)}{1-\omega_1}\right). \tag{54}$$

Remark 8. *Based on (54), one can observe that the asymptotic ESR of x_2 tends to be a constant independent of ρ at the high-SNR region.*

Similarly, based on (11), one can observe that the ergodic rate of x_5 tends to a constant independent on ρ since γ^{x_5} tends to a constant independent on ρ when $\rho \to \infty$. Moreover, increasing $a_1^{t_2}$ results in decreasing of γ^{x_5} since less power is allocated for x_5.

Based on (43), (44), and (47), the asymptotic expressions for the lower bound of the ESSR is obtained as

$$\bar{C}_{\mathrm{ESSR}}^{\mathrm{L},\rho\to\infty} \approx \ln(a_S\nu\rho\lambda_{SU_N}) + \ln\left(a_1^{t_2}\rho\lambda_{SU_N}\right) + \ln\left(\frac{\rho\lambda_{RU_F}}{2}\right). \tag{55}$$

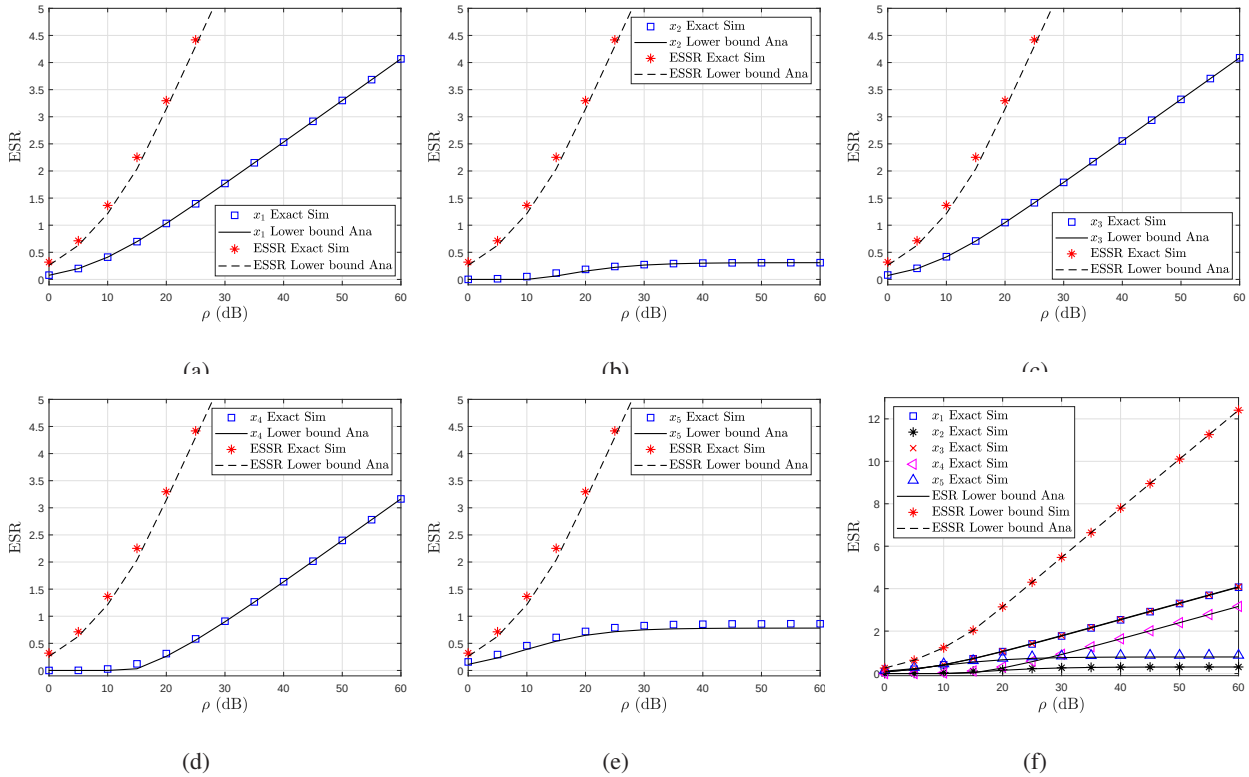


Fig. 2: ESRs and ESSR versus ρ.

V. Simulation Results and Discussions

In this section, simulation and analysis results are presented to validate the effectiveness of the proposed secure scheme. The effects of system parameters on secure performance of the considered system, such as transmit SNR, average channel gains, power ratio coefficient, and power allocation coefficients, are investigated. Without loss of generality, the parameters in the simulation and analysis are set as $\lambda_{SU_N} = \lambda_{RU_F} = 1$, $\lambda_{SR} = 0.7$, $\lambda_{RU_N} = \lambda_{U_N U_F} = 0.8$, $\nu = 2$, $a_S = 0.2$, and $a_1^{t_2} = 0.5$. 'Sim', 'Ana', and 'Asy' in all the figures denote the simulation, numerical, and asymptotic results. Since there are five ESRs in the expression of ESSR, we present the effect of each system parameter on the ESRs and ESSR. To prove the superiority of the proposed scheme, two conventional schemes are considered as benchmarks:

1) A CDRT system based on NOMA without PNC ('Ben1'): S broadcasts downlink superimposed signals $\sqrt{a_S P_S}x_1 + \sqrt{\bar{a}_S P_S}x_2$ and U_F emits jamming $\sqrt{P_U}z_1$ in the first slot (t_1), R amplifies received signals and forwards to U_F in the second slot (t_2), U_N and U_F broadcast uplink NOMA signals $\sqrt{a_1^{t_2} P_U}x_3 + \sqrt{\bar{a}_1^{t_2} P_U}z_2$ and $\sqrt{P_U}x_4$ in the third slot (t_3), and in

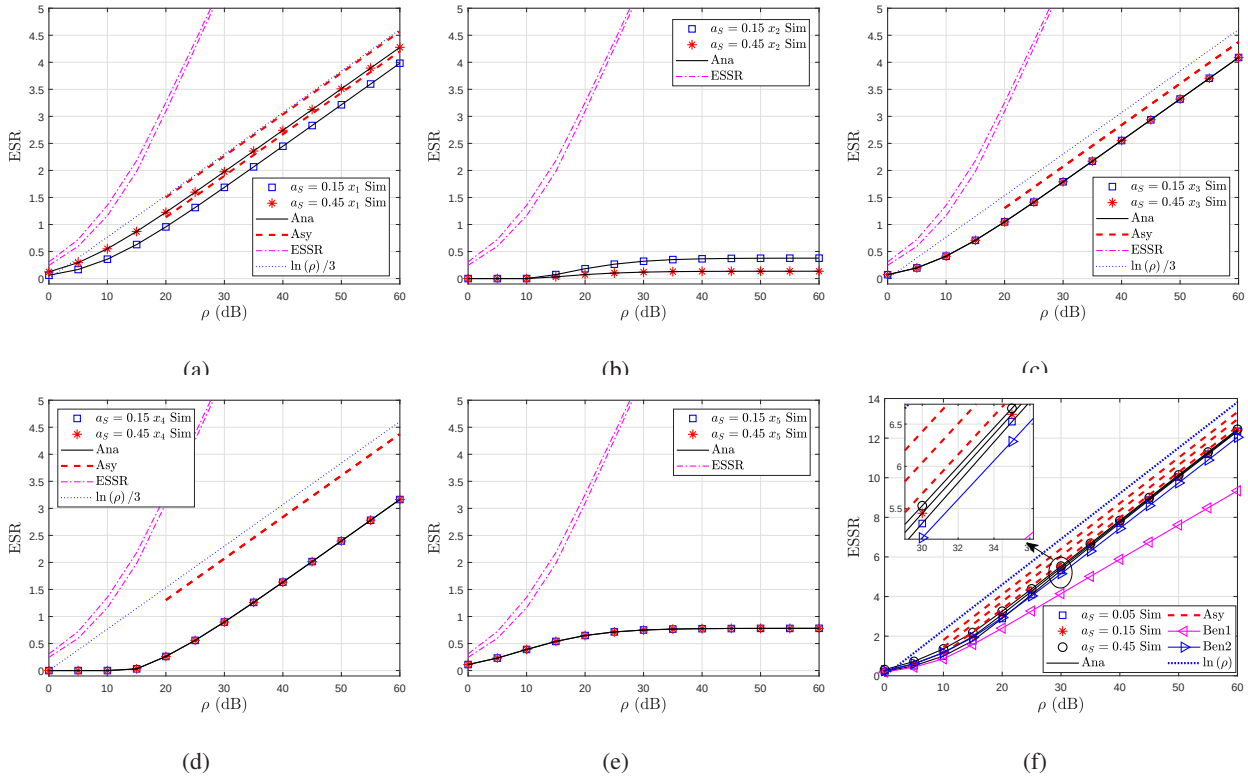


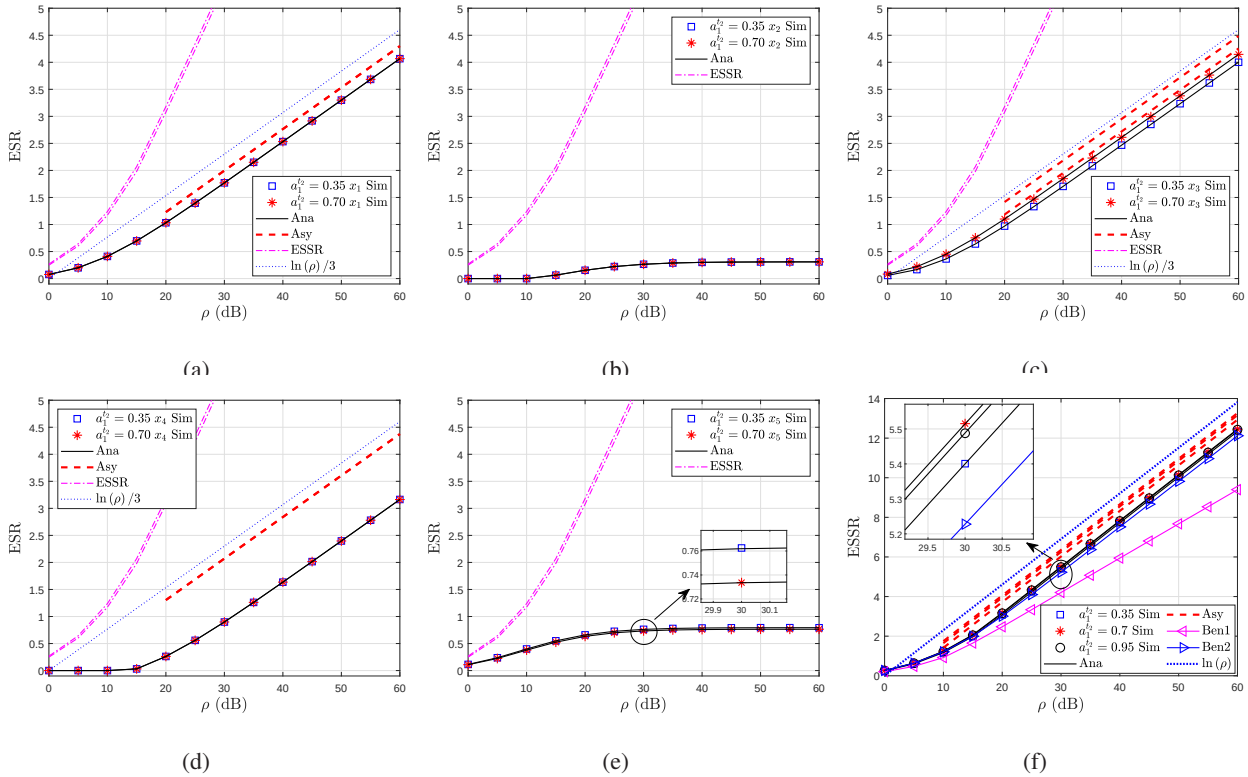
Fig. 3: ESRs and ESSR for varying ρ and a_S.

final slot (t_4) U_N sends a new uplink signal x_5, meanwhile R amplifies received signals x_4.

2) A CDRT system based on NOMA and PNC without jamming signal ('Ben2'): There are three slots in each fading block. S broadcasts superimposed signals $\sqrt{a_S P_S}x_1 + \sqrt{\bar{a}_S P_S}x_2$ in the first slot (t_1), U_N and U_F transmit $\sqrt{P_U}x_3$ and $\sqrt{P_U}x_4$ in the second slot (t_2), and in the third slot (t_3) R amplifies and broadcasts the received signals in previous two time slots and U_N transmits $\sqrt{P_U}x_5$ to S.

Fig. 2 shows simulation results for the exact ESR and numerical results for the lower bound of ESR versus ρ. It is found that simulation and lower bound results of x_1 - x_4 match perfectly, which represent approximate the ESR of the considered system by using the lower bound is feasible.

Fig. 3 plots the effect of ρ and a_S on the simulation results for the lower bound of ESRs and ESSR. One can observe that simulation and numerical results match perfectly to verify the correctness of the analysis, and it is apparent that ESSR increases with increasing ρ and a_S. This



(a) (b) (c)

(d) (e) (f)

Fig. 4: ESRs and ESSR for varying ρ and $a_1^{t_2}$.

is because the legitimate rates always increase and the eavesdropping rates initially increase and subsequently remain constant with increasing ρ. Different from ρ, a_S only affects the ESR of x_1 and x_2. The ESR of x_1 gets better and remain increasing with increasing a_S, correspondingly the ESR of x_2 gets worse with increasing a_S. Due to poor channel gain and the presence of inter-user interference, the slope of the decrease in the ESR of x_2 is less than the slope of the increase in the ESR of x_1, thus the ESSR increases with increasing a_S.

Fig. 4 demonstrates the lower bound of ESRs and ESSR vs transmit SNR ρ for varying $a_1^{t_2}$. It can be observed that the ESSR of the proposed scheme increases with an increase in ρ. Different from a_S, one can observe the ESSR increases initially and subsequently decreases with increasing $a_1^{t_2}$. This verifies that there is an optimal $a_1^{t_2}$ to achieve the optimal performance, which confirms the result in *Remark 4*.

Fig. 5 presents the impact of ρ for varying λ_{RU_N} on the lower bound of ESRs and ESSR. We find that the effect of λ_{RU_N} on the ESSR in the lower-ρ region is different from that in the higher-ρ region. The lower λ_{RU_N}, the larger ESSR in the lower-ρ region while the lower λ_{RU_N},

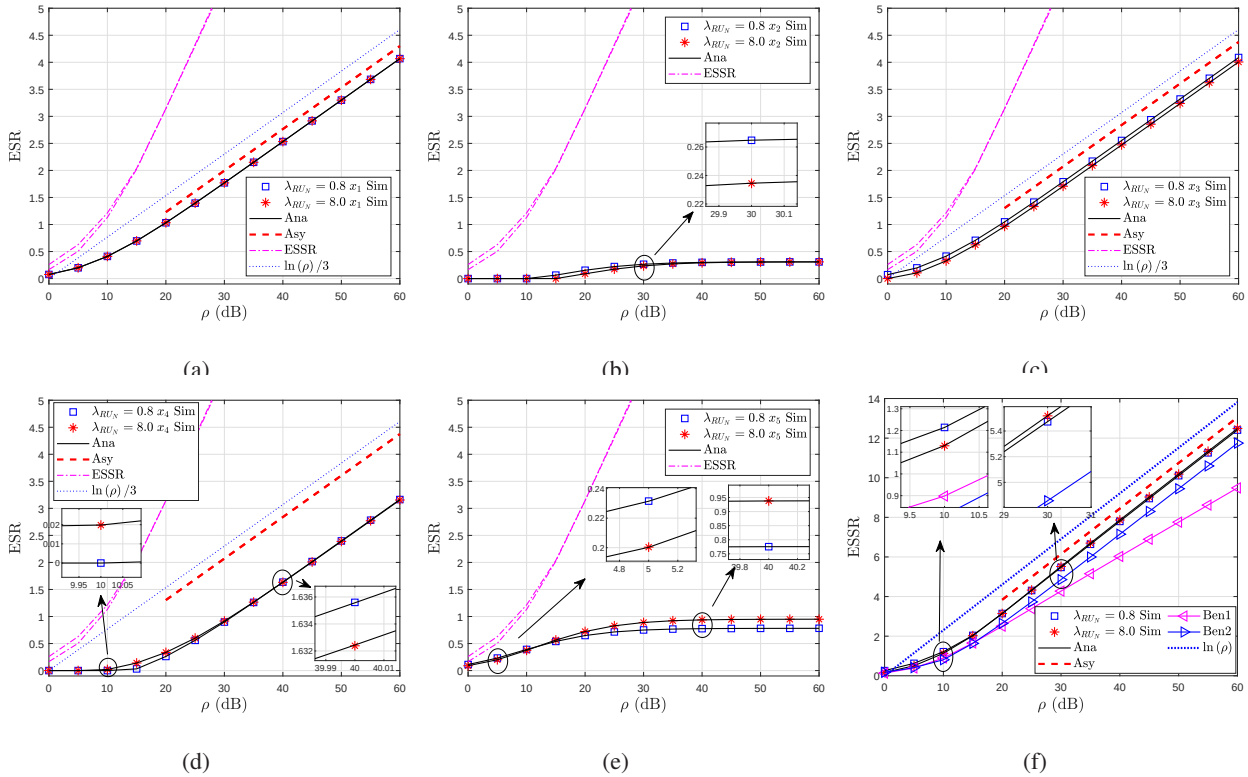


Fig. 5: ESRs and ESSR for varying ρ and λ_{RU_N}.

the lower ESSR in the higher-ρ region. This is because the quality of R-U_N link has a different influence on the ESR of x_3 and x_4. Lower λ_{RU_N} results in a poor eavesdropping rate of x_3, which leads to a higher ESR of x_3. However, lower λ_{RU_N} results in the poor jamming quality of z_2, which leads to decreasing in ESR of x_4, even to zero. In the higher-ρ region, not only the jamming influence of z_2 is strong but also amplifying coefficient decreases, then both γ^{x_4} and $\gamma_R^{x_4}$ become worse. The ESR of x_3 is improved since the eavesdropping and jamming quality at R are enhanced simultaneously.

Fig. 6 shows the lower bound of ESRs and ESSR with varying ρ and λ_{RU_F}. It is found that the ESSR with high λ_{RU_F} in the lower-ρ region outperforms that with lower λ_{RU_F}. In the lower-ρ region, the ESSR with low λ_{RU_F} outperforms that with high λ_{RU_F}. This is because ESRs of x_1 and x_3 play significant roles in the lower-ρ region, while the variation of ESR of x_4 dominates in the higher-ρ region. ESRs of x_1 and x_3 increase and ESR of x_4 decreases as increases of λ_{RU_F}.

Fig. 7 gives the comparison of the lower bound of ESRs and ESSR versus ρ with varying ν.

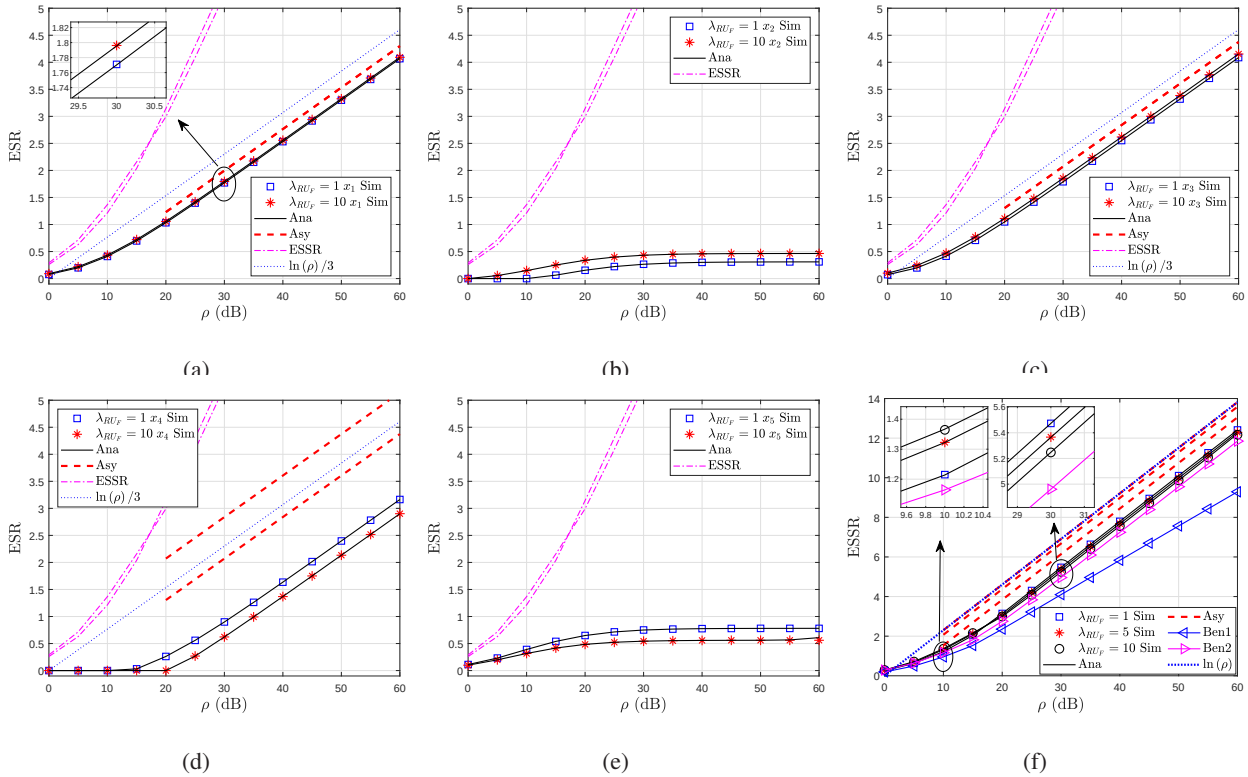


Fig. 6: ESRs and ESSR for varying ρ and λ_{RU_F}.

A trend is that ESSR increases with an increase in ρ and ν, which represent that the ESSR with higher ν (higher ρ_S) outperforms that with lower ν, which is easy understand since increasing transmit SNR can enhance the secrecy performance. The ESR of x_1 predominates in this scenario and ESR of x_3 almost is independent on ν. From Figs. 3 - 7, it is easily observed that the scaling law of proposed scheme is obtained by asymptotic results.

Fig. 8 plots the simulation results for the lower bound of ESRs and ESSR for varying a_S and λ_{RU_F} with $\rho = 20$ dB. It can be found that the ESSR increases with increasing a_S while the rate of growth decreases. This is because the ESR of x_1 increases with increasing a_S and dominates. Moreover, ESSR with lower λ_{RU_F} outperforms that with higher λ_{RU_F} in lower-a_S region. This is because ESRs of x_1, x_2, and x_3 increase and ESRs of x_4 and x_5 decrease as increasing of λ_{RU_F}. ESR of x_4 dominates in lower-a_S region and ESR of x_1 dominates in higher-a_S region.

Fig. 9 shows the effect from $a_1^{t_2}$, λ_{RU_F}, and λ_{RU_N} on the lower bound of ESRs and ESSR. One can find there is an optimal $a_1^{t_2}$ to maximize the ESSR and the optimal $a_1^{t_2}$ depends on λ_{RU_F} and λ_{RU_N}. This is because ESR of x_5 is dominant in lower-$a_1^{t_2}$ region and ESR of x_3

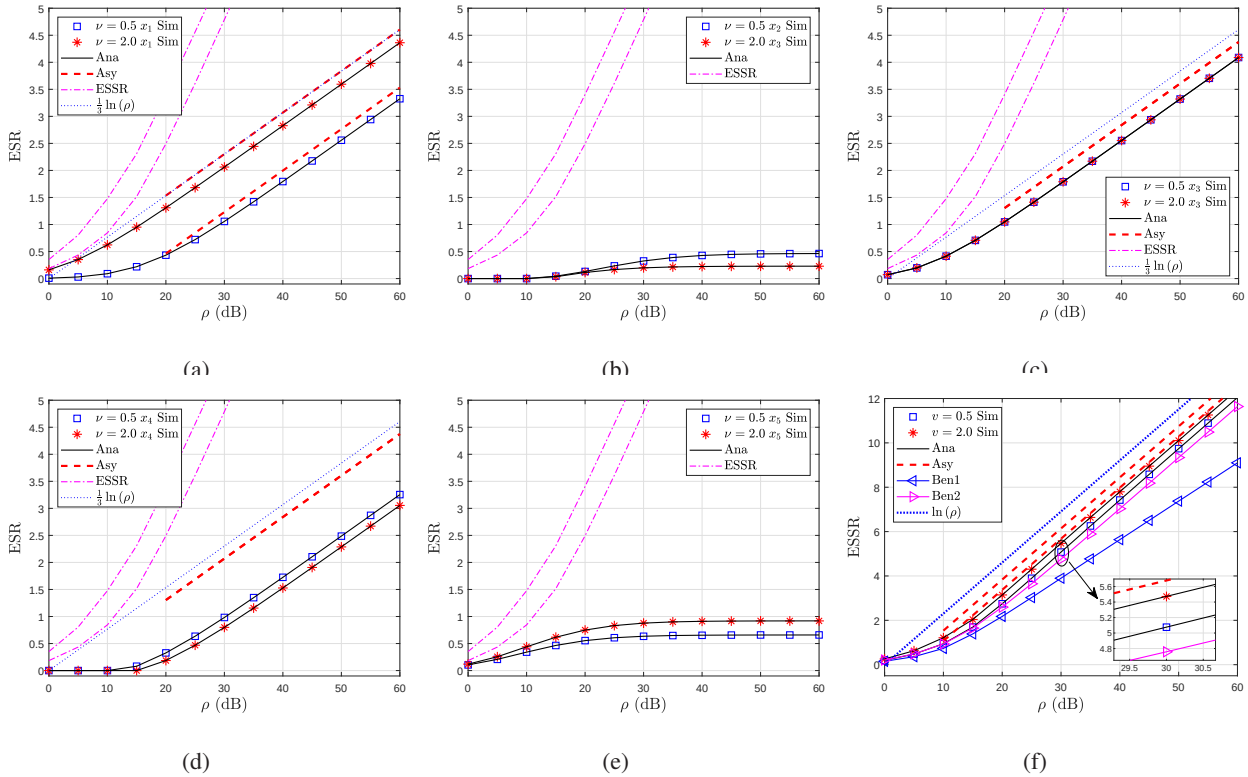


Fig. 7: ESRs and ESSR for varying ρ and ν.

is dominant in higher-$a_1^{t_2}$ region. As $a_1^{t_2}$ increases, ESR of x_3 increases to the maximum then decreases. From Figs. 3 - 9, we observe that simulation and numerical results match perfectly to verify the correctness of our analysis. Compared to the Benchmarks, the proposed scheme achieves higher secure performance.

VI. Conclusion

In this paper, we proposed a new scheme called NOMA-CDRT-PNC to provide reliable and secure communication for the CDRT system with uplink and downlink transmission. Cooperative jamming and inter-user interference prevented information leakage against the untrusted relay and NOMA and PNC schemes are utilized to enhance SE. To characterize the security performance of the proposed schemes, we derived the expressions for lower bounds of the exact and asymptotic ESSR. The effects of system parameters on the ESSR were analyzed in detail. Simulations were provided to verify the correctness of the analytical results. The results showed that the proposed scheme obtained better security performance than conventional schemes. An interesting work is

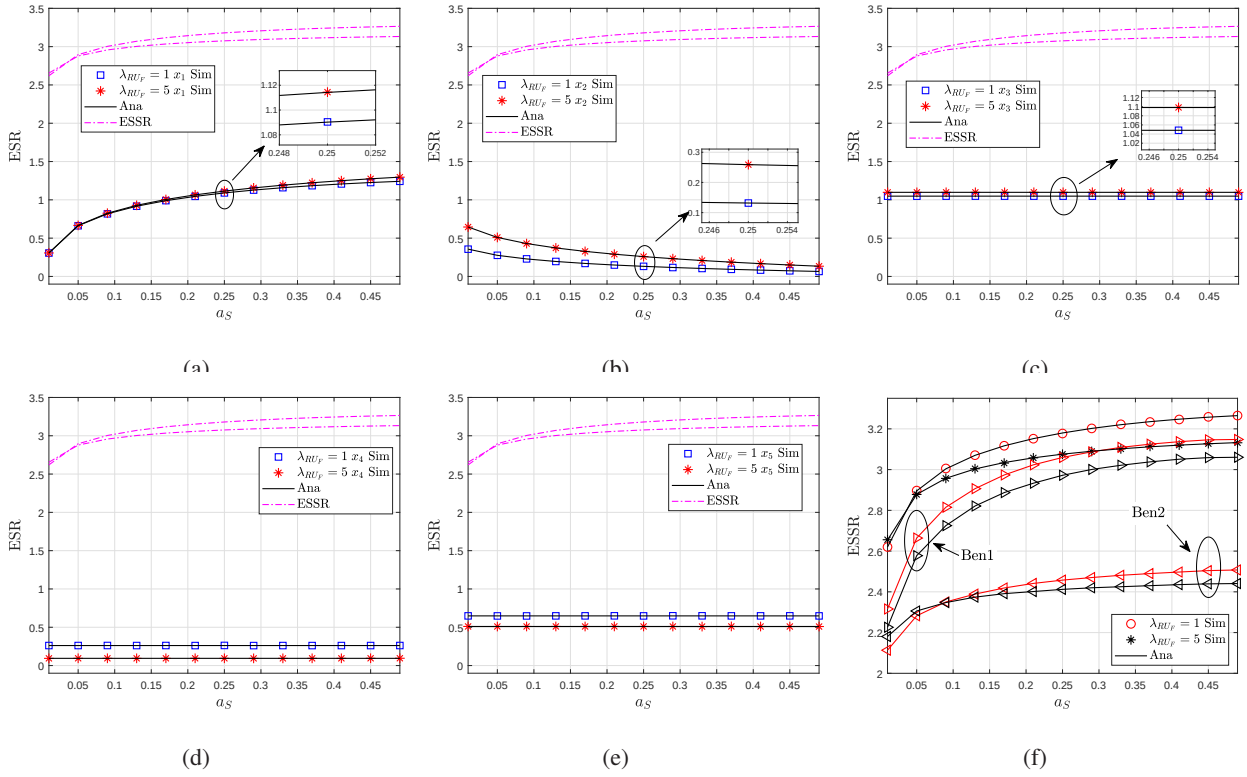


Fig. 8: ESRs and ESSR for varying ρ and ν.

to investigate the secrecy performance of CDRT systems with imperfect SIC and imperfect CSI, which will be part of our future work.

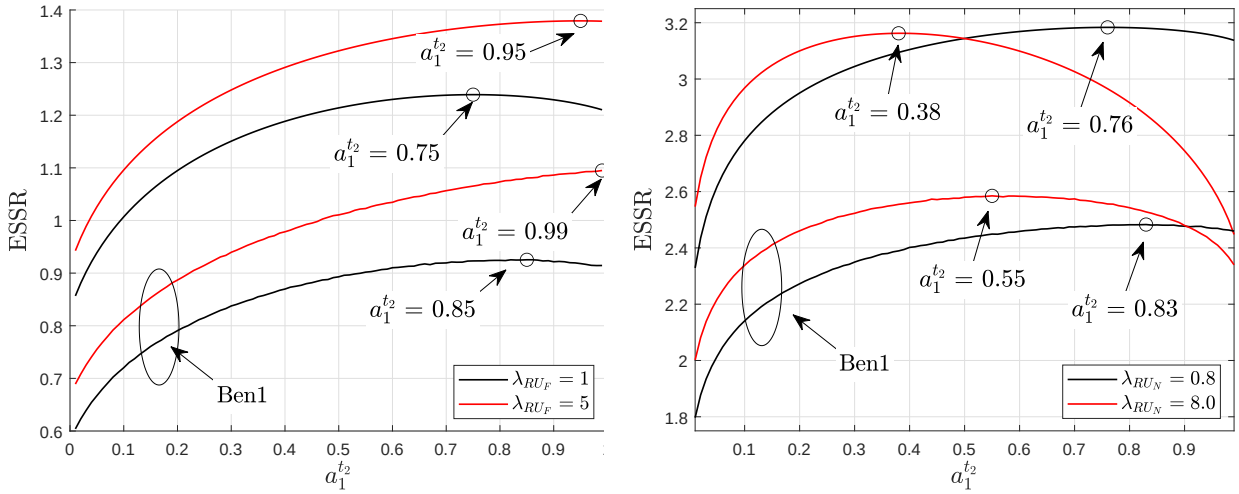
Appendix A
Derivation of $\phi_5(a,b)$

Utilizing $\ln(y) = \frac{dy^s}{ds}\big|_{s=0}$, $\phi_5(a,b)$ is expressed as

$$\begin{aligned}\phi_5(a,b) &= \int_0^\infty \frac{e^{-by}}{ay+1}\ln(y)\,dy \\ &= \int_0^\infty \frac{e^{-by}}{ay+1}\frac{dy^s}{ds}\bigg|_{s=0} dy \\ &= \frac{d}{ds}\int_0^\infty \frac{y^s e^{-by}}{ay+1}dy\bigg|_{s=0}.\end{aligned} \tag{56}$$

Then utilizing [31, (10), (11), (21)] and [24, (9.31.2), (9.31.5)], we obtain

$$\begin{aligned}\int_0^\infty \frac{y^s e^{-by}}{ay+1}dy &= \int_0^\infty y^s G_{1,1}^{1,1}\left[ay\left|\begin{matrix}0\\0\end{matrix}\right.\right] G_{0,1}^{1,0}\left[by\left|\begin{matrix}-\\0\end{matrix}\right.\right] dy \\ &= a^{-s-1}G_{2,1}^{1,2}\left[\begin{matrix}1,1+s\\1+s\end{matrix}\middle|\frac{a}{b}\right].\end{aligned} \tag{57}$$



(a) ESSR for varying λ_{RU_F} with $\rho = 10$ dB.

(b) ESSR for varying λ_{RU_N} with $\rho = 20$ dB.

Fig. 9: ESRs and ESSR for varying $a_1^{t_2}$.

Then utilizing residue theorem, we have

$$\begin{aligned} G_{2,1}^{1,2}\left(\begin{smallmatrix}1,1+s\\1+s\end{smallmatrix}\middle|\frac{a}{b}\right) &= \frac{1}{2\pi i}\int_L \Gamma(p)\Gamma(-s+p)\Gamma(s+1-p)\left(\frac{a}{b}\right)^p dp \\ &= \lim_{p\to s}(p-s)\Gamma(p)\Gamma(-s+p)\Gamma(s+1-p)\left(\frac{a}{b}\right)^p \\ &+ \lim_{p\to 0} p\Gamma(p)\Gamma(-s+p)\Gamma(s+1-p)\left(\frac{a}{b}\right)^p + \mathcal{O}(a^s) \\ &\simeq \lim_{p\to s}\Gamma(p)\Gamma(-s+p+1)\Gamma(s+1-p)\left(\frac{a}{b}\right)^p \\ &+ \lim_{p\to 0}\Gamma(-s+p)\Gamma(s+1-p)\left(\frac{a}{b}\right)^p \\ &= \Gamma(s)\left(\frac{a}{b}\right)^s + \Gamma(-s)\Gamma(s+1), \end{aligned} \tag{58}$$

where $\mathcal{O}(a^s)$ denotes higher order terms. Substituting (58) into (56), we have

$$\phi_5(a,b) = a^{-1}\frac{d\Theta(s)}{ds}\bigg|_{s=0}, \tag{59}$$

where $\Theta(s) = b^{-s}\Gamma(s) + a^{-s}\Gamma(-s)\Gamma(s+1)$. By utilizing [24, (8.322)], we have

$$\Gamma(s) = \frac{e^{-\mathrm{C}s}}{s}\prod_{k=1}^{\infty}\left(1+\frac{s}{k}\right)^{-1}e^{\frac{s}{k}}. \tag{60}$$

By substituting $e^{-\mathrm{C}s}$ with its taylor series, $e^{-\mathrm{C}s}=1-\mathrm{C}s+\frac{\mathrm{C}^2s^2}{2}+\mathcal{O}\left(s^2\right)$, (60) is rewritten as

$$\begin{aligned}\Gamma\left(s\right) &\overset{s\to 0}{=} \frac{1-\mathrm{C}s+\frac{\mathrm{C}^2s^2}{2}+\mathcal{O}\left(s^2\right)}{s}\\ &=\frac{1}{s}-\mathrm{C}+\frac{\mathrm{C}^2}{2}s+\mathcal{O}\left(s\right)\\ &=\frac{1}{s}-\mathrm{C}+\omega_3,\end{aligned} \tag{61}$$

where $\omega_3=\frac{\mathrm{C}^2}{2}s+\mathcal{O}\left(s\right)$. Similarly, we have $\Gamma\left(-s\right)=-\frac{1}{s}-\mathrm{C}-\omega_3$. Then $\Theta\left(s\right)$ is rewritten as

$$\begin{aligned}\Theta\left(s\right) &= b^{-s}\left(\frac{1}{s}-\mathrm{C}+\omega_3\right)+a^{-s}\left(\frac{1}{-s}-\mathrm{C}-\omega_3\right)\Gamma\left(s+1\right)\\ &=\underbrace{\frac{b^{-s}}{s}-\frac{a^{-s}\Gamma\left(s+1\right)}{s}}_{I_3}+\underbrace{\omega_3 b^{-s}-\mathrm{C}b^{-s}-\mathrm{C}a^{-s}\Gamma\left(s+1\right)-\omega_3 a^{-s}\Gamma\left(s+1\right)}_{I_4}.\end{aligned} \tag{62}$$

Defining $f_1\left(s\right)=b^{-s}$ and $f_2\left(s\right)=a^{-s}\Gamma\left(s+1\right)$, then Taylor series expansions of $f_1\left(s\right)$ and $f_2\left(s\right)$ at $s=0$ are expressed as

$$\begin{aligned}f_1\left(s\right) &= b^{-s}\\ &=f_1\left(0\right)+f_1'\left(0\right)\frac{s}{1!}+f_1''\left(0\right)\frac{s^2}{2!}+\mathcal{O}\left(s^2\right)\\ &=1-\ln\left(b\right)s+\frac{\ln^2\left(b\right)s^2}{2}+\mathcal{O}\left(s^2\right),\end{aligned} \tag{63}$$

and

$$\begin{aligned}f_2\left(s\right) &= a^{-s}\Gamma\left(s+1\right)\\ &=f_2\left(0\right)+f_2'\left(0\right)\frac{s}{1!}+f_2''\left(0\right)\frac{s^2}{2!}+\mathcal{O}\left(s^2\right)\\ &=1+f_2'\left(0\right)s+f_2''\left(0\right)s^2+\mathcal{O}\left(s^2\right),\end{aligned} \tag{64}$$

respectively, where $f_2'\left(0\right)$ and $f_2''\left(0\right)$ are given as

$$\begin{aligned}f_2'\left(0\right) &= \frac{d}{ds}\left(a^{-s}\Gamma\left(s+1\right)\right)|_{s=0}\\ &=-\ln\left(a\right)a^{-s}\Gamma\left(s+1\right)+a^{-s}\Gamma\left(s+1\right)\varphi_0\left(s+1\right)|_{s=0}\\ &=\mathrm{C}-\ln\left(a\right),\end{aligned} \tag{65}$$

and

$$\begin{aligned}f_2''\left(0\right) &= \frac{d^2}{ds^2}\left(a^{-s}\Gamma\left(s+1\right)\right)|_{s=0}\\ &=\left(a^{-s}\right)''\Gamma\left(s+1\right)+2\left(a^{-s}\right)'\left(\Gamma\left(s+1\right)\right)'+a^{-s}\left(\Gamma\left(s+1\right)\right)''|_{s=0}\\ &=\left(\ln\left(a\right)\right)^2\Gamma\left(1\right)-2\ln\left(a\right)\Gamma'\left(1\right)+\Gamma''\left(1\right)\\ &=\ln^2\left(a\right)+2\mathrm{C}\ln\left(a\right)+\psi^{(1)}\left(1\right)+\mathrm{C}^2,\end{aligned} \tag{66}$$

respectively, where $\Gamma'(1)=\Gamma(1)\psi^{(0)}(1)=-\mathrm{C}$, $\Gamma''(1)=\psi^{(1)}(1)+(\Gamma'(1))^2=\psi^{(1)}(1)+\mathrm{C}^2$, and $\psi^{(k)}(x)$ is the polygamma function as defined by [24, (8.363.8)].

Then I_3 is obtained as

$$\begin{aligned} I_3 &= \frac{1-\ln(b)\,s+\frac{\ln^2(b)}{2!}s^2}{s}-\frac{1+f_2'(0)\,s+\frac{f_2''(0)}{2}s^2}{s} \\ &= -\ln(b)+\frac{s\ln^2(b)}{2}-f_2'(0)-f_2''(0)\frac{s}{2}. \end{aligned} \tag{67}$$

Substituting (65) and (66) into (67), ${I_3}'$ is obtained as

$$\begin{aligned} {I_3}' &= \frac{\ln^2(b)}{2!}-\frac{{f''}_2(0)}{2} \\ &= \frac{\ln^2(b)}{2}-\frac{\ln^2(a)+2\mathrm{C}\ln(a)+\psi^{(1)}(1)+\mathrm{C}^2}{2}. \end{aligned} \tag{68}$$

Similar as (68), we obtain

$$\begin{aligned} {I_4}'|_{s=0} &= \left(-\mathrm{C}b^{-s}+\omega_3 b^{-s}-\mathrm{C}a^{-s}\Gamma(s+1)\ -\omega_3 a^{-s}\Gamma(s+1)\right)' \\ &= (\mathrm{C}-\omega_3)\,b^{-s}\ln(b)+\frac{\mathrm{C}^2}{2}b^{-s}+\left(\ln(a)-\varphi^{(0)}(s+1)\right)\mathrm{C}a^{-s}\Gamma(s+1) \\ &\quad -\frac{\mathrm{C}^2a^{-s}\Gamma(s+1)}{2}\left(1+\left(\varphi^{(0)}(s+1)-\ln(a)\right)s\right) \\ &= \mathrm{C}\ln(ab)+\mathrm{C}^2. \end{aligned} \tag{69}$$

Substituting (68) and (69) into (59), we obtain

$$\begin{aligned} \phi_5(a,b) &= \frac{1}{a}\left({I_3}'+{I_4}'|_{s=0}\right) \\ &= \frac{\ln^2(b)}{2a}-\frac{\ln^2(a)+2\mathrm{C}\ln(a)+\psi^{(1)}(1)+\mathrm{C}^2}{2a}+\frac{\mathrm{C}}{a}\ln(ab)+\frac{\mathrm{C}^2}{a} \\ &= \frac{1}{2a}\ln\left(\frac{b}{a}\right)\ln(ab)-\frac{1}{2a}\psi^{(1)}(1)+\frac{\mathrm{C}}{a}\ln(b)+\frac{\mathrm{C}^2}{2a}. \end{aligned} \tag{70}$$

REFERENCES

[1] Z. Ding, X. Lei, G. K. Karagiannidis, and R. Schober, "A survey on non-orthogonal multiple access for 5G networks: Research challenges and future trends," *IEEE J. Sel. Areas Commun.*, vol. 35, no. 10, pp. 2181-2195, Oct. 2017.

[2] L. Lv, J. Chen, Q. Ni, and Z. Ding, "Design of cooperative non-orthogonal multicast cognitive multiple access for 5G systems: User scheduling and performance analysis," *IEEE Trans Commun.*, vol. 65, no. 6, pp. 2641-2656, Jun. 2017.

[3] J.-B. Kim and I.-H. Lee, "Non-orthogonal multiple access in coordinated direct and relay transmission," *IEEE Commun. Lett.*, vol. 19, no. 11, pp. 2037-2040, Nov. 2015.

[4] X. Li, Y. Chen, P. Xue, G. Lv, and M. Shu, "Outage performance for satellite-assisted cooperative NOMA systems with coordinated direct and relay transmission," *IEEE Commun. Lett.*, vol. 24, no. 10, pp. 2285-2289, Oct. 2020.

[5] G. Pandey and A. Jaiswal, "Coordinated and non-coordinated direct-and-relay transmission: A signal space diversity approach," *IEEE Commun. Lett.*, vol. 25, no. 6, pp. 1825-1829, Jun. 2021.

[6] T.-T. Nguyen, T.-V. Nguyen, T.-H. Vu, and D. B. da Costa, "IoT-based coordinated direct and relay transmission with non-orthogonal multiple access," *IEEE Wireless Commun. Lett.*, vol. 10, no. 3, pp. 503-507, Mar. 2021.

[7] T.-T. Nguyen, T.-H. Vu, T.-V. Nguyen, and D. B. da Costa, "Underlay cognitive NOMA-based coordinated direct and relay transmission," *IEEE Wireless Commun. Lett.*, vol. 10, no. 4, pp. 854-858, Apr. 2021.

[8] T.-H. Vu, T.-V. Nguyen, D. B. da Costa, and S. Kim, "Performance analysis and deep learning design of underlay cognitive NOMA-based CDRT networks with imperfect SIC and co-channel interference," *IEEE Wireless Commun. Lett.*, vol. 69, no. 12, pp. 8159-8174, Dec. 2021.

[9] L. Zou, J. Chen, L. Lv, and B. He, "Capacity enhancement of D2D aided coordinated direct and relay transmission using NOMA," *IEEE Commun. Lett.*, vol. 24, no. 10, pp. 2128-2132, Oct. 2020.

[10] Y. Xu, B. Li, N. Zhao, Y. Chen, G. Wang, Z. Ding, and X. Wang, "Coordinated direct and relay transmission with NOMA and network coding in Nakagami-m fading channels," *IEEE Trans. Commun.*, vol. 69, no. 1, pp. 207-222, Jan. 2021.

[11] Y. Xu, J. Cheng, G. Wang, and V. C. M. Leung, "Adaptive coordinated direct and relay transmission for NOMA networks: A joint downlink-uplink scheme," *IEEE Trans. Wireless Commun.*, vol. 20, no. 7, pp. 4328-4346, Jul. 2021.

[12] M. Yang, J. Chen, R. Q. Hu, and L. Yang, "Non-orthogonal multiple access with coordinated direct and user-assisted transmission," *IEEE Commun. Lett.*, vol. 25, no. 1, pp. 264-268, Jan. 2021.

[13] Y. Liao, L. Song, Z. Han, and Y. Li, "Full duplex cognitive radio: A new design paradigm for enhancing spectrum usage," *IEEE Commun. Mag.*, vol. 53, no. 5, pp. 138-145, May. 2015.

[14] Q. Si, M. Jin, Y. Chen, and N. Zhao, "Performance analysis of spatial modulation aided NOMA with full-duplex relay," *IEEE Trans. Veh. Technol.*, vol. 69, no. 5, pp. 5683-5687, May. 2020.

[15] X. Pei, H. Yu, M. Wen, and S. Mumtaz, "NOMA-based coordinated direct and relay transmission with a half-duplex/full-duplex relay," *IEEE Trans. Commun.*, vol. 68, no. 11, pp. 6750-6760, Nov. 2020.

[16] X. Chen, G. Liu, Z. Ma, and X. Zhang, "Optimal power allocations for non-orthogonal multiple access over 5G full/half-duplex relaying mobile wireless networks," *IEEE Trans. Wireless Commun.*, vol. 18, no. 1, pp. 77-92, Jan. 2019.

[17] L. Lv, Z. Li, H. Ding, Y. Zhoy, and J. Chen, "Secure coordinated direct and untrusted relay transmissions via interference engineering," *Sci. China Inf. Sci.*, doi: 10.1007/s11432-021-3259-0, May 2021.

[18] L. Lv, H. Jiang, Z. Ding, L. Yang, and J. Chen, "Secrecy-enhancing design for cooperative downlink and uplink NOMA with an untrusted relay," *IEEE Trans. Commun.*, vol. 68, no. 3, pp. 1698-1715, Mar. 2020.

[19] L. Lv, Z. Li, H. Ding, and J. Chen, "Secure NOMA and OMA coordinated transmission schemes in untrusted relay networks," *Sci. China Inf. Sci.*, vol. 64, Article number: 209302, doi: 10.1007/s11432-020-3015-y, Oct. 2021.

[20] L. Lv, F. H. Zhou, J. Chen, and N. Al-Dhahir, "Secure cooperative communications with an untrusted relay: A NOMA-inspired jamming and relaying approach," *IEEE Trans. Inf. Forensics Security.*, vol. 14, no. 12, pp. 3191-3205, Dec. 2019.

[21] B. Li, Y. Zou, J. Zhou, F. Wang, W. Cao, and Y.-D. Yao, "Secrecy outage probability analysis of friendly jammer selection aided multiuser scheduling for wireless networks," *IEEE Trans. Commun.*, vol. 67, no. 5, pp. 3482-3495, May. 2019.

[22] T.-X. Zheng, H.-M. Wang, D. W. K. Ng, and J. Yuan, "Physical-layer security in the finite blocklength regime over fading channels," *IEEE Trans. Wireless Commun.*, vol. 19, no. 5, pp. 3405-3420, May. 2020.

[23] M. Bloch, J. Barros, M. R. D. Rodrigues, and S. W. McLaughlin, "Wireless information-theoretic security," *IEEE Trans. Inf. Theory*, vol. 54, no. 6, pp. 2515-2534, Jun. 2008.

[24] I. S. Gradshteyn and I. M. Ryzhik, *Table of Integrals, Series, and Products*, 7th edition. Academic Press, 2007.

[25] V. S. Adamchik and O. I. Marichev, "The algorithm for calculating integrals of hypergeometric type functions and its realization in REDUCE system," in *Proc. the international symposium on Symbolic and algebraic computation (ISSAC '90)*, Tokyo, Japan, Aug. 1990, pp. 212-224.

[26] A. M. Mathai, R. K. Saxena, and H. J. Haubold, *The H-Function: Theory and Applications*. Berlin, Germany: Springer, 2010.

[27] H. Lei, I. S. Ansari, G. Pan, B. Alomair, and M.-S. Alouini, "Secrecy capacity analysis over α-μ fading channels," *IEEE Commun. Lett.*, vol. 21, no. 6, pp. 1445-1448, Jun. 2017.

[28] M. Yan, Q. Chen, X. Lei, T. Q. Duong, and P. Fan, "Outage probability of switch and stay combining in two-way amplify-and-forward relay networks," *IEEE Wireless Commun. Lett.*, vol. 1, no. 4, pp. 296-299, Aug. 2012.

[29] C. Zhang, Y. Liu, W. Yi, Z. Qin, and Z. Ding, "Semi-grant-free NOMA: Ergodic rates analysis with random deployed users," *IEEE Wireless Commun. Lett.*, vol. 10, no. 4, pp. 692-695, Apr. 2021.

[30] X. Yue and Y. Liu, "Performance analysis of intelligent reflecting surface assisted NOMA networks," *IEEE Trans. Wireless Commun.*, vol. 21, no. 4, pp. 2623-2636, Oct. 2021.

[31] V. S. Adamchik and O. I. Marichev, "The algorithm for calculating integrals of hypergeometric type functions and its realization in REDUCE system," in *Proc. the international symposium on Symbolic and algebraic computation (ISSAC '90)*, Tokyo, Japan, Aug. 1990, pp. 212-224.